

# Material Matters™

Volume 10, Number 2

**ALDRICH**  
Materials Science



## Carbon in Multiple Dimensions

### **POLYMER-SORTED SEMICONDUCTING CARBON NANOTUBES**

for Transistors and Solar Cells

### **NOVEL GRAPHENE-BASED NANOSTRUCTURES:**

Production, Functionalization, and Engineering

### **GRAPHENE-BASED COMPOSITES**

and Their Unique Renewable Energy Applications

### **GRAPHENE FIELD EFFECT TRANSISTORS**

for Biological and Chemical Sensors

### **FLUORESCENCE QUENCHING MICROSCOPY:**

Imaging Two-dimensional Materials

## Graphene and Carbon Nanomaterials

## Introduction

Welcome to the second issue of *Material Matters*™ for 2015, focusing on graphene and carbon nanomaterials. Innovation of nanomaterials continues to stimulate rapid growth in the nano community. With unique electrical, optical and mechanical properties, carbon nanomaterials have been attracting a great deal of interest in such diverse areas as photonics, optoelectronics, and sensors, as well as energy generation and storage. This widespread interest in graphene and carbon nanotubes is driven by the expectation that the performance of these new materials will soon challenge the dominance of well-established technologies. This issue reviews and highlights the promising applications and technologies employing graphene and carbon nanotubes, as well as some recent breakthroughs in synthesis, characterization, and application.



Jia Choi, Ph.D.  
Aldrich Materials Science

In the first article, Prof. Michael S. Arnold et al. (USA) highlight a promising separation method for improving the performance of single-walled carbon nanotubes (SWCNTs) in electronic devices. This sorting method uses polyfluorene to separate metallic SWCNTs from semiconducting SWCNTs, and yields semiconducting SWCNT purities greater than 99.9%. The authors emphasize advances in isolation and processing to improve the performance of SWCNT devices and advance knowledge of 1D material properties.

Prof. Vincenzo Palermo et al. (Italy), in the second article, provide a brief overview on the chemical exfoliation, functionalization, and engineering of new original nanostructures based on graphene. They review the tailored synthesis of graphene in a variety of forms ranging from simple, soluble sheets to hierarchical architectures where 2D graphene sheets are assembled into 3D bulk materials or foams for applications in electronics, composites, energy storage, or catalysis.

The third article by Dr. Andrew Y. Wang et al. (USA) reviews a novel process that can be used to conjugate various metals and metal oxides to graphene, as well as fabricate graphene-based hybrid devices for supercapacitors, direct methanol fuel cells, and use in photocatalytic water splitting applications. The authors discuss how introducing graphene as a substrate, selecting an environmentally benign solvent, controlling the size of metal/metal oxide nanocrystals (NCs) without aggregation, and eliminating the use of surfactants and stabilizers can significantly improve the properties of as-made graphene metal and metal oxide hybrids, as well as enhance the performance and stability of graphene-based hybrid devices.

In the fourth article, Dr. Victoria Tsai and Mr. Bruce Willner (USA) focus on the emerging graphene-based field effect transistor (GFET) sensors for biological or chemical detection. The unique properties, advantages, and perspective of graphene materials for use in sensing are discussed.

In the final article, Prof. Jiaying Huang et al. (USA) highlight fluorescence quenching microscopy (FQM), a versatile imaging technique for graphene-based materials and other emerging 2D materials. The principles and techniques of FQM are described, and its advantages and capabilities are emphasized.

As always, each article in this publication is accompanied by a list of relevant materials available from Aldrich® Materials Science. For additional product information, visit [aldrich.com/matsci](http://aldrich.com/matsci). Please bother us with your new product suggestions, as well as thoughts and comments for *Material Matters*™ at [matcsi@sial.com](mailto:matcsi@sial.com).

## About Our Cover

Carbon-based nanomaterials possess extraordinary electrical, thermal, chemical, and mechanical properties that make them unique among nanomaterials. These exceptional properties have allowed carbon nanomaterials to find application in such diverse areas as electronics, energy, and biomedical fields. The cover art for this issue expresses carbon nanomaterials using hexagonal patterns, reflecting the orientation of carbon atoms within carbon nanotubes, nanoribbons, and graphene. Potential applications that use carbon nanomaterials are depicted within the hexagons. Aldrich® Materials Science is proud to serve researchers with a large variety of innovative carbon nanomaterials as well as the highest level of quality and product information to inform and enable research and development efforts.

# Material Matters™

Vol. 10, No. 2

**Aldrich Materials Science  
Sigma-Aldrich Co. LLC**  
6000 N. Teutonia Ave.  
Milwaukee, WI 53209, USA

### To Place Orders

Telephone 800-325-3010 (USA)  
FAX 800-325-5052 (USA)

International customers, contact your local Sigma-Aldrich office  
([sigma-aldrich.com/worldwide-offices](http://sigma-aldrich.com/worldwide-offices)).

### Customer & Technical Services

Customer Inquiries 800-325-3010  
Technical Service 800-325-5832  
SAFC® 800-244-1173  
Custom Synthesis 800-244-1173  
Flavors & Fragrances 800-227-4563  
International 314-771-5765  
24-Hour Emergency 314-776-6555  
Safety Information [sigma-aldrich.com/safetycenter](http://sigma-aldrich.com/safetycenter)  
Website [sigma-aldrich.com](http://sigma-aldrich.com)  
Email [aldrich@sial.com](mailto:aldrich@sial.com)

### Subscriptions

Request your FREE subscription to *Material Matters*:

Phone 800-325-3010 (USA)  
Mail Attn: Marketing Communications  
Aldrich Chemical Co., Inc  
Sigma-Aldrich Co. LLC  
P.O. Box 2060  
Milwaukee, WI 53201-2060  
Website [aldrich.com/mm](http://aldrich.com/mm)  
Email [sams-usa@sial.com](mailto:sams-usa@sial.com)

### Online Versions

Explore previous editions  
of *Material Matters* [aldrich.com/materialmatters](http://aldrich.com/materialmatters)



Now available for your iPad®  
[aldrich.com/mm](http://aldrich.com/mm)

*Material Matters* (ISSN 1933-9631) is a publication of Aldrich Chemical Co., Inc. Aldrich is a member of the Sigma-Aldrich Group.

©2015 Sigma-Aldrich Co. LLC. All rights reserved. SIGMA, SAFC, SIGMA-ALDRICH, and ALDRICH, are trademarks of Sigma-Aldrich Co. LLC, registered in the US and other countries. *Material Matters* is a trademark of Sigma-Aldrich Co. LLC. iPad is a registered trademark of Apple Inc. IsoNanotubes-M, IsoNanotubes-S, PureTubes, and SuperPureTubes are trademarks of NanoIntegrus, Inc. V2V is a trademark of Chasm Technologies, Inc. Plexcore is a registered trademark of Plextronics, Inc. Rieke is a registered trademark of Rieke Metals, Inc. CoMoCAT and SWeNT are registered trademarks of SouthWest NanoTechnologies, Inc. Sigma brand products are sold through Sigma-Aldrich, Inc. Purchaser must determine the suitability of the product(s) for their particular use. Additional terms and conditions may apply. Please see product information on the Sigma-Aldrich website at [www.sigmaaldrich.com](http://www.sigmaaldrich.com) and/or on the reverse side of the invoice or packing slip.

## Table of Contents

### Articles

Polymer-sorted Semiconducting Carbon Nanotubes for Transistors and Solar Cells	37
Novel Graphene-based Nanostructures: Production, Functionalization, and Engineering	45
Graphene-based Composites and Their Unique Renewable Energy Applications	53
Graphene Field Effect Transistors for Biological and Chemical Sensors	60
Fluorescence Quenching Microscopy: Imaging Two-dimensional Materials	64

### Featured Products

<b>Carbon Nanotubes (CNTs)</b> A selection of single, double, and multi-walled CNTs and single-walled CNT inks	41
<b>Fullerenes</b> A selection of C <sub>60</sub> , C <sub>70</sub> and their derivatives	43
<b>Graphite</b> A list of graphite for use in graphene and graphene oxide production	50
<b>Graphene Oxide and Reduced Graphene Oxide</b> A list of graphene oxide powder, dispersion and film and reduced graphene oxide	50
<b>Precursors of 2D Materials</b> A selection of 2D material precursors	50
<b>Organic Molecules for use in Processing Graphene</b> A selection of polycyclic aromatic hydrocarbons, porphyrin dyes, and polythophenes	50
<b>Graphene Nanocomposites</b> A selection of graphene and reduced graphene oxide-based nanocomposites	57
<b>Graphene</b> A list of graphene, graphene nanoplatelets, graphene inks and graphene nanoribbons	58
<b>Nanoparticles</b> A selection of nanoparticles for use in nanocomposites	59
<b>Graphene Films and Graphene Field Effect Transistor (GFET) Chip</b> A list of graphene films and GFET chip for use in electronics and sensors	62
<b>Fluorescent Dyes</b> A selection of fluorescent dyes for use in graphene and 2D materials imaging	66
<b>Polymers for Fluorescence Quenching Microscopy</b> A selection of polyvinylpyrrolidones and poly(methyl methacrylate)s	67

## Your Materials Matter



*Bryce P. Nelson*

Bryce P. Nelson, Ph.D.  
Aldrich Materials Science Initiative Lead

We welcome fresh product ideas. Do you have a material or compound you wish to see featured in the Aldrich® Materials Science line? If it is needed to accelerate your research, it matters. Send your suggestion to [matsci@sial.com](mailto:matsci@sial.com) for consideration.

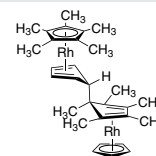
Prof. Seth Marder and Dr. Steve Barlow of Georgia Tech (USA) recommended the addition of pentamethylcyclopentadienyl cyclopentadienyl rhodium dimer (**Aldrich Prod. No. 795615**) to our catalog for use as an n-dopant for organic semiconductors, and in particular for the surface doping of materials such as graphene. This compound is one of a class of dimeric sandwich compounds.<sup>1,2</sup> It is relatively stable in air, but can reduce acceptor materials with electron affinities down to ca. 3 eV with relative ease during fabrication processes such as co-sublimation or solution processing.<sup>1</sup> Upon reaction, the dimers contribute two electrons to the acceptor materials forming two molecules of the corresponding monomeric cations (pentamethylrhodocenium in this case). The pentamethylrhodocene dimer in particular has been applied to the solution-processed surface doping of single-layer graphene. This was accomplished by immersion of the substrate in a 2.5 mM solution of the dimer for 10 min, followed by rinsing with additional solvent, leading to a reduction of the work function of the CVD graphene by over 1 eV (to ca. 2.8 eV) and a significant increase in its conductivity.<sup>3</sup>

### References

- (1) Guo, S.; Kim, S. B.; Mohapatra, S. K.; Qi, Y.; Sajoto, T.; Kahn, A.; Marder, S. R.; Barlow, S. *Adv. Mater.* **2012**, *24*, 699.
- (2) Mohapatra, S. K.; Fonari, A.; Risko, C.; Yesudas, K.; Moudgil, K.; Delcamp, J. H.; Timofeeva, T. V.; Brédas, J.-L.; Marder, S. R.; Barlow, S. *Chem. Eur. J.* **2014**, *20*, 15385.
- (3) Paniagua, S. A.; Baltazar, J.; Sojoudi, H.; Mohapatra, S. K.; Zhang, S.; Henderson, C. L.; Graham, S.; Barlow, S.; Marder, S. R. *Mater. Horiz.* **2014**, *1*, 1111.

### Pentamethylcyclopentadienyl cyclopentadienyl rhodium dimer

[RhCp\*<sub>2</sub>]<sub>2</sub>; 1,1,1,1,1-Pentamethylrhodocene dimer  
C<sub>30</sub>H<sub>40</sub>Rh<sub>2</sub> FW 606.45



Used as n-dopant

**795615-25MG**

25 mg

# TRANSPARENT CONDUCTIVE CNT INKS

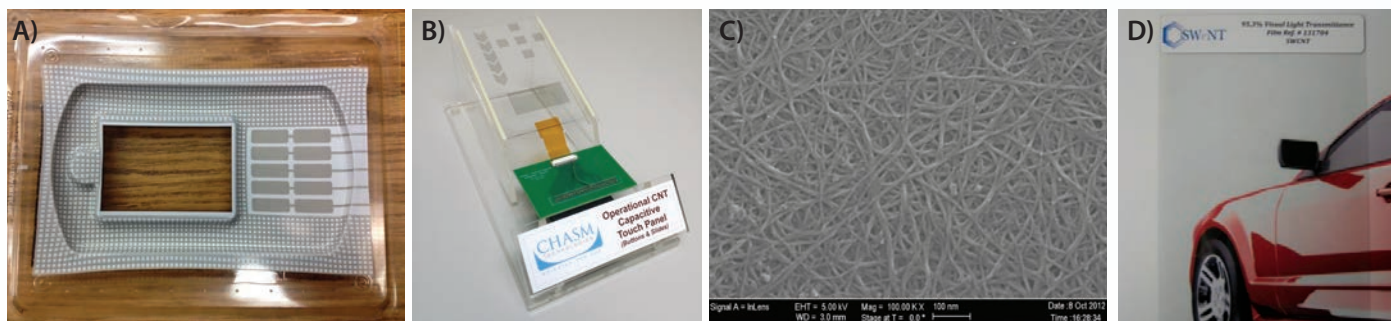
Printable • Environmentally Stable • Stretchable

Formulated using patented CoMoCAT™ CNTs, aqueous and solvent-based (V2V™) conductive inks are setting a new standard for transparent conductor performance in applications where durability and environmental stability are paramount.

## V2V™: Print. Dry. Done.

Conductive CNT Ink Systems are optimized for screen printing:

- Dries quickly, evenly at low temperature
- Contains no surfactants or electrically active dispersants, binders<sup>1</sup>
- Adheres strongly to common screen printing substrates



A) Thermoformed CNT touch sensor prototype, B) Capacitive CNT touch screen array, C) TEM scan of rod-coated CNT network (~10 mg/mm<sup>2</sup>), D) CNT TCF at 95% VLT.

## SWeNT® Conductive Inks

Description	Purpose	Sheet Resistance <sup>2</sup>			Aldrich Prod. No.	
		85% VLT	90% VLT	92% VLT		
AC100	SWCNT in aqueous surfactant solution	Spray Coating	137 Ω/sq.	237 Ω/sq.	330 Ω/sq.	791490
AC200	SWCNT in aqueous surfactant solution	Meyer-Rod/Slot-Die Coating	166 Ω/sq.	251 Ω/sq.	317 Ω/sq.	791504
VC101	SWCNT in proprietary solvent system (V2V)	Screen Printing	783 Ω/sq.	1,466 Ω/sq.	2,206 Ω/sq.	792462

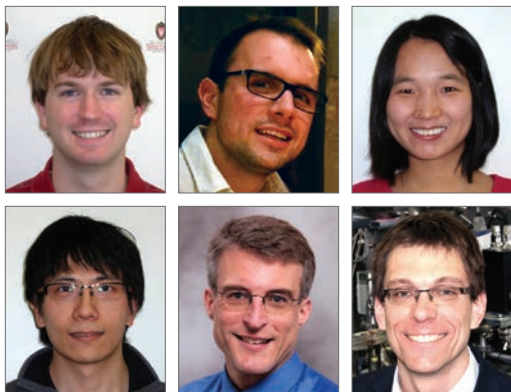
1. V2V inks (e.g., VC101) contain electrically inert sulfonated tetrafluoroethylene (Nafion).

2. SR measurements for AC100, 200 taken with top coat.

For detailed product information on SWeNT® Conductive Inks, visit [aldrich.com/swnt](http://aldrich.com/swnt)

# POLYMER-SORTED SEMICONDUCTING CARBON NANOTUBES

## FOR TRANSISTORS AND SOLAR CELLS



Matthew J. Shea,<sup>1</sup> Gerald J. Brady,<sup>1</sup> Juan Zhao,<sup>1,2</sup> Meng-Yin Wu,<sup>3</sup> Harold T. Evensen,<sup>3</sup> Michael S. Arnold<sup>1\*</sup>

<sup>1</sup>Department of Materials Science and Engineering, University of Wisconsin-Madison, USA

<sup>2</sup>School of Optoelectronic Information, University of Electronic Science and Technology of China, China

<sup>3</sup>Department of Electrical and Computer Engineering, University of Wisconsin-Madison, USA

\*Email: michael.arnold@wisc.edu

## Introduction

Single-walled carbon nanotubes (SWCNTs) are promising materials for use in the active channel of field-effect transistors (FETs), photoabsorbing layers of solar cells and photodetectors because of their ultrafast charge transport mobility,<sup>1</sup> tunable near-infrared band gaps,<sup>2</sup> and strong optical absorptivity.<sup>3</sup> Substituting traditional semiconductors with semiconducting SWCNTs (s-SWCNTs) has the potential to pave the way for advances in a number of applications: high performance computation, high bandwidth and high efficiency wireless communications, wearable devices, and renewable energy.

One substantial challenge in developing these applications using SWCNTs is their electronic heterogeneity. As-synthesized SWCNTs contain a mixture of both metallic SWCNTs (m-SWCNTs) and s-SWCNTs at a ratio of 1:2. The presence of m-SWCNTs limits the performance of electronic and optoelectronic devices by creating electrical short-circuit pathways and rapidly quenching photoexcitations in nearby s-SWCNTs.

In the last decade there have been significant advances in the post-synthetic sorting and isolation of s-SWCNTs. This article highlights one of the most promising sorting systems, polyfluorene derivatives. This material is capable of isolating s-SWCNTs to purities greater than 99.9% and also sorting SWCNTs by their diameter and bandgap, both of which are determined by the  $(n,m)$  chirality of each SWCNT. We have exploited the exceptional electronic-type purity of s-SWCNTs that have been prepared using polyfluorenes in order to harness the extraordinary properties of s-SWCNTs in conventional transistors, in flexible and stretchable transistors, and in photovoltaic devices.

## Separations

A number of promising methods have been developed to separate s-SWCNTs from mixtures of m- and s-SWCNTs, including column chromatography,<sup>4</sup> DNA-sorting,<sup>5</sup> density gradient ultracentrifugation,<sup>6</sup> and two-phase separation.<sup>7</sup> Methods based on the use of conjugated polymers to sort SWCNTs by electronic-type are perhaps the most promising. Nish et al.<sup>8</sup> identified the s-SWCNT selectivity of a family of aromatic polyfluorenes, most notably poly[9,9-dioctylfluorene-2,7-diyl] (PFO) (Aldrich Prod. No. 571652). Using simple, easily scaled, one-pot processing, they were able to isolate several  $(n,m)$  chiralities of s-SWCNTs from a polydisperse mixture of SWCNTs with diameters ranging from 0.8–1.2 nm. Spectra of similarly isolated SWCNT solutions are shown in Figure 1.

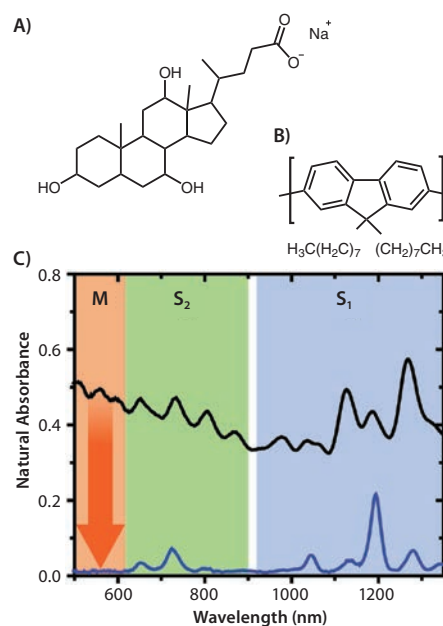


**Figure 1.** Chemical structures of (A) sodium cholate and (B) PFO. (C) The absorption spectra of SWCNTs isolated by sonication in aqueous sodium cholate solution (black) and PFO solution in toluene (blue). Regions containing the spectral signatures of S<sub>1</sub> (blue shaded), S<sub>2</sub> (green), and metallic (orange) are identified. Importantly, the PFO-sorted SWCNTs are completely free of m-SWCNT absorption signatures.

Sodium cholate surfactant (Sigma Prod. No. 27029) (Figure 1A) solubilizes both m- and s-SWCNTs, evident from the metallic absorption signatures near 500 nm. PFO (Figure 1B) selects only specific  $(n,m)$  s-SWCNTs while dispersing almost no m-SWCNTs. Subsequent studies have adjusted the diameter and chiral angle distribution of selectivity further by using starting SWCNT material with a narrower initial diameter distribution and through the addition of alternating copolymer units to the PFO backbone. Among these selective copolymers, poly[(9,9-dioctylfluorenyl-2,7-diyl)-alt-co-(6,6'-(2,2'-bipyridine))] (PFO-BPy) was shown to have significant selectivity for the (6,5) nanotubes<sup>9</sup> from the CoMoCAT synthetic process (Aldrich Prod. No. 773735) as well as a range of chiralities of nanotubes with diameters near 1.5 nm<sup>10</sup> from the arc-discharge synthetic process (Aldrich Prod. No. 698695). A number of other conjugated polymers and copolymers have also demonstrated various degrees of selectivity.<sup>11–14</sup>

The selectivity mechanism of these polymers is not well understood, although it is known that the backbone constituents and alkyl side-chain length<sup>13</sup> have a drastic effect on the SWCNT diameter, chiral angle, and electronic-type selectivity. In our group's work, we explored the conformation and binding coefficient of PFO on the surface of three different diameters of SWCNTs as a function of PFO concentration in the dispersion.<sup>15</sup> Similar methods may be used to explore the selectivity of newly developed selective polymers for niche chirality-specific isolation. The effectiveness of the separation of s-SWCNTs via PFO derivatives is exceptional, beyond the sensitivity of current metrology tools. We have characterized the electronic type of 5,519 SWCNTs isolated by PFO-BPy using field effect transistor measurements and have yet to find a single m-SWCNT, indicating semiconducting type purity of at least 99.98%.<sup>16</sup> With further refinements in processing and characterization, s-SWCNT purities exceeding 99.9999% (less than 1 ppm m-SWCNT) may be feasible.

## Transistors

High-purity s-SWCNTs are an appealing channel material for various types of field-effect transistors because of their high charge transport mobility and current carrying capacity in addition to their solution-processability and excellent mechanical resilience.<sup>17,18</sup> A schematic of a basic back-gated FET is shown in Figure 2A. The s-SWCNTs are top-contacted by palladium electrodes and are lying flat on a SiO<sub>2</sub>/Si substrate, which serves to electrostatically modulate the channel conductance. Important parameters for characterizing FET performance are the conductance of the channel when the gate is open ("on"), and the on/off ratio, which is the ratio of the "on" state conductance to the conductance when the gate is closed ("off"). The on-conductance of an FET is typically normalized to the width of the device and is affected by parameters such as the length of the FET channel, the quality of the s-SWCNTs, the source and drain contacts, and the s-SWCNT alignment. The on/off ratio is primarily determined by how well the channel can be switched off. m-SWCNTs cannot be turned off, and a low on/off ratio is observed when m-SWCNTs either directly bridge the channel or form a percolating network that bridges the channel.

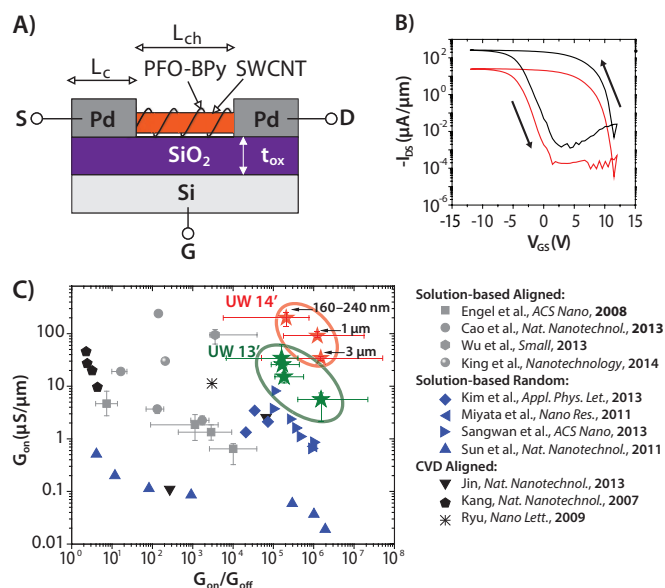


**Figure 2.** SWCNT FET architecture and performance. **A)** Schematic of a single SWCNT FET. **B)** Current-voltage characteristics of an aligned SWCNT FET at source drain bias of  $-1$  V (black) and  $-0.1$  V (red). **C)** Comparison of state-of-the-art SWCNT FET performance to the performance of SWCNT FETs presented in this work (red and green stars). Adapted with permission from Reference 16, copyright 2014, American Chemical Society.

Even if m-SWCNTs are present, it is possible to achieve high on/off ratio FETs under certain conditions. One approach has been to implement random networks of SWCNTs, which operate in a percolation regime enabling some immunity to sparse m-SWCNTs if they do not form a percolating pathway from source to drain. These SWCNT FETs can achieve high on/off ratios of  $\sim 10^7$ , however the on-conductance is typically less than  $10 \mu\text{S}/\mu\text{m}$ . Such conductance for a  $1 \mu\text{m}$  wide network is lower than the  $\sim 30 \mu\text{S}$  that can be achieved for a single nanotube SWCNT FET due to long channel lengths, network sparsity, and lack of alignment.<sup>19–21</sup> To increase on-conductance, researchers have developed approaches to controllably place and align SWCNTs into densely packed arrays.

One approach to the fabrication of aligned SWCNT FETs involves the direct growth of aligned SWCNTs via chemical vapor deposition. One challenge with this approach is that the as-grown SWCNT arrays are a mixture of electronic types, and the m-SWCNTs must be burned away.<sup>22</sup> Another challenge is that the density of the SWCNTs is also relatively low and it is, therefore, difficult to achieve high normalized conductance, although multiple growth and transfer approaches may overcome this problem.<sup>22,23</sup> Several groups developed solution-based methods for depositing aligned arrays of sorted s-SWCNTs. The varied approaches included Langmuir-Blodgett<sup>24</sup> and Langmuir-Schaefer<sup>25</sup> methods, dielectrophoretic techniques,<sup>26</sup> and evaporative self-assembly.<sup>27,28</sup> While each of these methods has its strengths, better control of the packing density is necessary. Ultrahigh density arrays ( $>1,000$  tubes/ $\mu\text{m}$ ) were demonstrated using the Langmuir-Schaefer approach, resulting in an on-conductance as high as  $250 \mu\text{S}/\mu\text{m}$ ; however, limitations in the purity resulted in an on/off ratio less than  $1,000$ .<sup>25</sup> In our work on high-performance SWCNT FETs, we showed that aligned ultrapure polyfluorene-sorted carbon nanotubes can achieve an on-conductance and on/off ratio of  $260 \mu\text{S}/\mu\text{m}$  and  $2 \times 10^5$ , respectively, in the same device.<sup>16</sup>

## Floating Evaporative Self-assembly of SWCNTs

In collaboration with Padma Gopalan's group at the University of Wisconsin-Madison, we recently demonstrated progress in increasing the on/off ratio and on-conductance of PFO-BPy sorted s-SWCNT FETs by aligning the SWCNTs with a technique we pioneered called Floating Evaporative Self-Assembly (FESA).<sup>29</sup> In FESA, a substrate is withdrawn from an aqueous sub-phase, onto which small droplets of SWCNT "ink" (namely, polymer-wrapped SWCNTs dissolved in chloroform) are delivered in the vicinity of the substrate (schematically depicted in **Figure 3A**). The ink spreads rapidly across the water surface and a thin film wets the substrate. This volatile ink film evaporates quickly and deposits a stripe of aligned, unbundled s-SWCNTs that spans the width of the substrate. The spacing of the stripes and the density of the SWCNTs within each stripe can be controlled through the deposition parameters. Scanning electron microscopy (SEM) and atomic force microscopy (AFM) images of aligned SWCNTs within a single stripe are presented in **Figures 3B–C**, where the AFM height profile indicates the film consists of an approximate monolayer of individualized SWCNTs. Overall, the result of FESA is the rapid deposition of SWCNTs into aligned arrays that can be adapted for scalable integration into a wide variety of microelectronic applications.

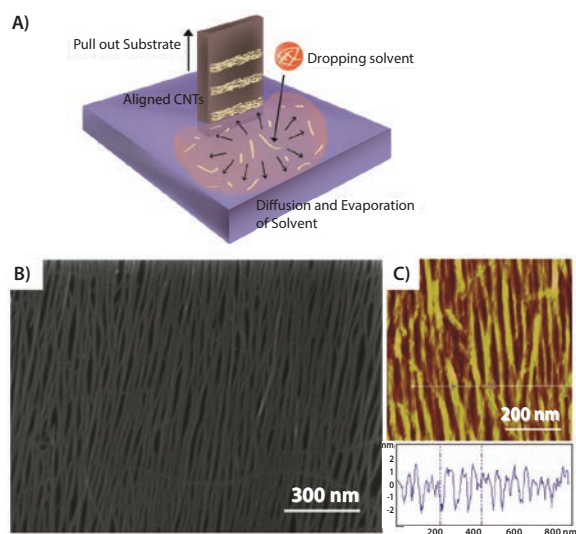


**Figure 3.** Alignment and film characteristics of SWCNTs prepared via Floating Evaporative Self-assembly. **A)** Schematic of the FESA experimental process. **B)** SEM image of aligned SWCNTs fabricated by FESA deposition. **C)** Atomic Force Microscopy tapping mode image of aligned SWCNTs. Inset height profile along the cross-section of the aligned SWCNTs indicates a monolayer of individualized SWCNTs. Adapted with permission from Reference 29, copyright 2014, American Chemical Society.

## High-performance Transistors

We leveraged our work on FESA to fabricate the highest performance nanotube FETs to date, using the on-conductance and on/off ratio as key metrics.<sup>16</sup> The source-drain current of an aligned SWCNT FET is plotted as a function of gate-voltage in **Figure 2B**. The measurement is used to extract values for on-conductance and on/off ratio of  $260 \mu\text{S}/\mu\text{m}$  and  $2 \times 10^5$ , respectively.<sup>16</sup> As shown in **Figure 2C**, compared to previous state-of-the-art SWCNT FETs, we achieved significant performance gains in on/off ratio and on-conductance.<sup>16,19,20,22,23,25,28,30–35</sup> We observed a 1,400-fold increase in on/off ratio compared to previous state-of-the-art SWCNT FETs with on-conductance per width of  $250 \mu\text{S}/\mu\text{m}$ . Likewise, 30–100 fold greater on-conductance per width was achieved when

compared to state-of-the-art high on/off ratio SWCNT FETs. The excellent performance of the devices resulted from the high semiconducting purity and the high degree of alignment of the SWCNT arrays. Moreover, the excellent performance was due to the SWCNTs remaining isolated and unbundled during their deposition, which minimized detrimental cross-talk between SWCNTs and improved the electrode/SWCNT contacts. Additionally, we used these FET arrays to measure the semiconducting purity based on the magnitude of the on/off ratio. These FETs contain 5,519 SWCNTs all having an on/off ratio greater than  $5 \times 10^3$ , indicating that the semiconducting purity is at least 99.98%. These results highlight the promise of aligned polyfluorene-sorted SWCNTs and FESA for next-generation thin film FET and computing applications.

## Flexible and Stretchable Transistors

The excellent mechanical resilience<sup>36</sup> of SWCNTs opens the door for their use in new types of electronic devices and circuits that are not confined to rigid substrates but can be integrated on flexible, elastomeric, or unconventional substrates like clothing, paper, or biological tissue that can flex, bend, and even stretch.<sup>37–39</sup> To fabricate highly flexible and stretchable thin film FETs, it is important to consider the mechanical behaviors of all of the components including the channel, electrodes, and dielectric, and the interfaces between them, under deformation. Our group fabricated highly stretchable FETs by depositing random networks of PFO sorted s-SWCNTs onto pre-stretched elastomer substrates and buckling the network thin films by releasing the strain.<sup>40</sup> The contacts are composed of buckled gold/chromium thin films, and a polymeric ionic conductor is used as a flexible dielectric. The FETs fabricated in this way can operate under strain of over 50% without sacrificing electrical performance in on/off ratio or mobility,<sup>40</sup> as shown in **Figure 4**.

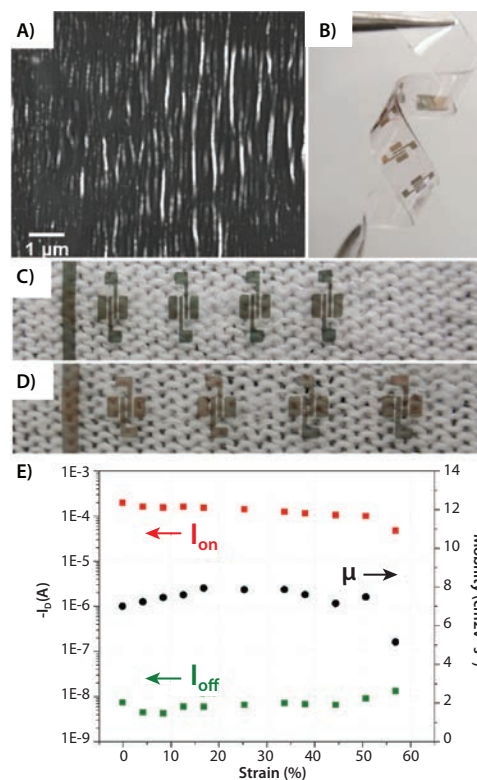


**Figure 4.** **A)** SEM image of buckled s-oSWCNT film after release of pre-strain and demonstration of **(B)** flexibility and **(C,D)** stretchability. **E)** On ( $I_{on}$ ) and off ( $I_{off}$ ) currents and mobility ( $\mu$ ) versus strain of the stretchable FETs. Adapted with permission from Reference 40, copyright 2014 American Chemical Society.

# Carbon Nanotube Optoelectronics

## Device Operation

s-SWCNTs are promising photoabsorbers for next-generation photovoltaic solar cells and photodetectors because they are strong optical absorbers with tunable bandgaps, transport energy and charge on ultrafast timescales, are relatively chemically stable, and are solution-processable. The application of s-SWCNTs as the efficient light-absorbing component of photovoltaic devices has only recently been possible with the advent of methods for eliminating m-SWCNTs, which otherwise are known to quench photoexcitations in nearby s-SWCNTs.

One challenge is that optical absorption in s-SWCNTs produces electron-hole pairs known as excitons. The electrons and holes in the excitons are bound to each other with an energy that is  $>100$  meV, significantly above thermal energy at room temperature, suppressing their spontaneous dissociation and separation into free charges that are needed to produce electrical energy.<sup>41</sup> We have shown that it is possible to overcome the exciton binding energy by pairing thin films of s-SWCNTs with other semiconductors to create heterojunctions.<sup>42</sup> The heterojunction must have a band offset exceeding the exciton binding energy to allow efficient exciton dissociation. For example, fullerene- $C_{60}$  (Aldrich Prod. Nos. 572500, 379646 and 483036) is an excellent electron acceptor for thin films of large bandgap polyfluorene-sorted s-SWCNTs, including (6,5), (7,5), (7,6), and (8,6) chiralities. The internal quantum efficiency (IQE), which quantifies the fraction of absorbed photons that result in separated electron-hole pairs that are collected at the device contacts at zero-bias, is  $>85\%$  for these species when the SWCNT film thickness is less than  $\sim 5$  nm.<sup>43</sup> The IQE of the SWCNT/ $C_{60}$  heterojunction decreases to less than 50% when the (8,7) and (9,7) SWCNTs are used due to a decreasing band offset and a lower driving force for exciton dissociation.<sup>44</sup>

Another factor that influences IQE is the exciton diffusion length. In a bilayer heterojunction device, photogenerated excitons must diffuse to the SWCNT/ $C_{60}$  heterointerface (where dissociation will take place) before the excitons recombine and are lost as heat. Excitons can diffuse either along the long-axis of SWCNTs (intra-tube) or transfer between SWCNTs (inter-tube). In solution-cast SWCNT films, the SWCNTs adopt a lying-down morphology. Exciton diffusion to the  $C_{60}$  layer must occur via inter-tube hopping. During inter-tube hopping, excitons tend to

hop from large to small bandgap species (i.e., downhill energy transfer). Because small bandgap nanotubes are less efficient donors and trap excitons, it is important to avoid them, in addition to avoiding m-SWCNTs. In a recent modeling study, we found that the chirality distribution of s-SWCNTs can significantly influence the exciton diffusion length,<sup>45</sup> with the longest exciton diffusion lengths predicted for films of nearly monochiral s-SWCNTs.

## Recent Advances

Using nearly monochiral films of (7,5) SWCNTs, Bindl et al. reported a monochromatic power conversion efficiency of 7.1% at the  $S_1$  transition of the (7,5) nanotube.<sup>46</sup> Later optimization by Shea et al. yielded a power conversion efficiency of nearly 1.0% (Figures 5A–D) under simulated solar irradiation (AM1.5G).<sup>47</sup> Of particular note is that the photoabsorbing SWCNT films driving the power conversion in these devices are only several nanometers thick. One may expect that an increase in SWCNT film thickness would yield a corresponding increase in power conversion efficiency. However, Bindl and Shea et al. noted that the optimized external quantum efficiency and power conversion lies at s-SWCNT film thickness of 5–8 nm. It is believed that the short inter-tube exciton diffusion length<sup>48</sup> (discussed previously) limits the maximum film thickness achievable before decreased exciton diffusion efficiency outweighs any increase in absorption obtained from a thicker film.

A common method to avoid the problem of short exciton diffusion length is to fabricate bulk or blended heterojunction devices where the acceptor material is never more than an exciton diffusion length away from a photogenerated exciton in the donor. Most polymer bulk heterojunction (BHJ) devices are fabricated by casting solutions containing both a polymer donor such as P3HT and a fullerene-derivative acceptor at similar concentration. One complication associated with replacing the common P3HT:fullerene BHJ with a SWCNT:fullerene analog is the relatively low solubility of PFO-wrapped SWCNTs compared to small molecule fullerene-derivative electron acceptors. Ye et al. developed one solution to this problem by fabricating s-SWCNT aerogels and filling the aerogels with a fullerene-derivative solution.<sup>49</sup> In this way, significantly higher optical density at the SWCNT transitions were achieved without limiting exciton diffusion pathways. Ye et al. reported a maximum AM1.5G power conversion efficiency of 1.7% (Figures 5E–H). Others have also recently reported exciting progress towards the use of s-SWCNTs in the light-absorbing components of solar cells<sup>50,51</sup> and photodetectors.<sup>52</sup>

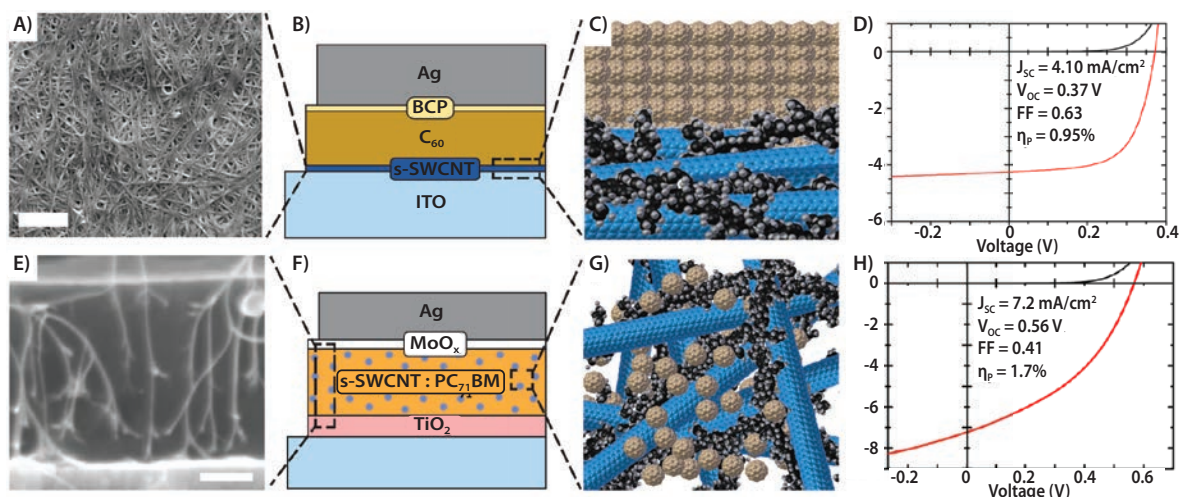


**Figure 5.** A) Scanning electron micrograph of a film of s-SWCNTs. The scale bar is 200 nm. B,C) Device schematic for bilayer s-SWCNT/ $C_{60}$  heterojunction solar cell. D) Bilayer solar cell performance under AM1.5G illumination. Adapted with permission from Reference 47, copyright 2013 American Institute of Physics. E) Cross-section micrograph of bulk heterojunction fabricated by intercalation of s-SWCNT aerogel by PC<sub>71</sub>BM. The scale bar is 100 nm. F,G) Device schematic for bulk heterojunction s-SWCNT:PC<sub>71</sub>BM solar cell. H) Solar cell performance under AM1.5G illumination. Adapted with permission from Reference 49, copyright 2014 Wiley.

## Conclusion

Polyfluorene sorting provides a simple, scalable method to achieve s-SWCNTs for electronic and optoelectronic applications. With electronic-type purity of at least 99.98%, s-SWCNTs isolated by this process are appealing materials for a number of next-generation electronic and optoelectronic devices. Our group has specialized in incorporating polyfluorene-sorted s-SWCNTs in high performance FETs, flexible and stretchable devices, and as the photoabsorbing material in solar cells and photodetectors. Advances in isolation and processing will continue to improve the performance of SWCNT-based devices and advance knowledge of the properties and behaviors of these one-dimensional materials.

## Acknowledgments

Support is acknowledged from the National Science Foundation (CMMI-1129802), the University of Wisconsin National Science Foundation Materials Research Science and Engineering Center (MRSEC) (DMR-1121288), the National Science Foundation (DMR-1350537), the U.S. Army Research Office (W911NF-12-1-0025), and the Air Force Office of Scientific Research (FA9550-12-1-0063). GJB also acknowledges support from the National Science Foundation Graduate Research Fellowship Program under Grant No. DGE-1256259.

## References

- Durkop, T.; Getty, S. A.; Cobas, E.; Fuhrer, M. S. *Nano Lett.* **2004**, *4*, 35.
- Weisman, R. B.; Bachilo, S. M. *Nano Lett.* **2003**, *3*, 1235.
- Avouris, P.; Freitag, M.; Perebeinos, V. *Nature Photonics* **2008**, *2*, 341.
- Liu, H. P.; Nishide, D.; Tanaka, T.; Kataura, H. *Nat. Commun.* **2011**, *2*.
- Zheng, M.; Jagota, A.; Semke, E. D.; Diner, B. A.; McLean, R. S.; Lustig, S. R.; Richardson, R. E.; Tassi, N. G. *Nature Materials* **2003**, *2*, 338.
- Arnold, M. S.; Green, A. A.; Hulvat, J. F.; Stupp, S. I.; Hersam, M. C. *Nat. Nanotechnol.* **2006**, *1*, 60.
- Khripin, C. Y.; Fagan, J. A.; Zheng, M. *J. Am. Chem. Soc.* **2013**, *135*, 6822.
- Nish, A.; Hwang, J. Y.; Doig, J.; Nicholas, R. J. *Nat. Nanotechnol.* **2007**, *2*, 640.
- Ozawa, H.; Ide, N.; Fujigaya, T.; Niidome, Y.; Nakashima, N. *Chem. Lett.* **2011**, *40*, 239.
- Mistry, K. S.; Larsen, B. A.; Blackburn, J. L. *ACS Nano* **2013**, *7*, 2231.
- Berton, N.; Lemasson, F.; Poschlad, A.; Meded, V.; Tristram, F.; Wenzel, W.; Hennrich, F.; Kappes, M. M.; Mayor, M. *Small* **2014**, *10*, 360.
- Wang, H.; Koleilat, G. I.; Liu, P.; Jimenez-Oses, G.; Lai, Y.-C.; Vosgueritchian, M.; Fang, Y.; Park, S.; Houk, K. N.; Bao, Z. *ACS Nano* **2014**, *8*, 2609.
- Gomulya, W.; Costanzo, G. D.; de Carvalho, E. J. F.; Bisri, S. Z.; Derenskiy, V.; Fritsch, M.; Frohlich, N.; Allard, S.; Gordiichuk, P.; Herrmann, A.; Marrink, S. J.; dos Santos, M. C.; Scherf, U.; Loi, M. A. *Adv. Mater.* **2013**, *25*, 2948.
- Lemasson, F.; Berton, N.; Tittmann, J.; Hennrich, F.; Kappes, M. M.; Mayor, M. *Macromolecules* **2012**, *45*, 713.
- Shea, M. J.; Mehlenbacher, R. D.; Zanni, M. T.; Arnold, M. S. *J. Phys. Chem. Lett.* **2014**, *5*, 3742.
- Brady, G. J.; Joo, Y.; Wu, M. Y.; Shea, M. J.; Gopalan, P.; Arnold, M. S. *ACS Nano* **2014**, *8*, 11614.
- Carbon Nanotube Electronics*, **2009**.
- Chau, R.; Doyle, B.; Datta, S.; Kavalieros, J.; Zhang, K. *Nature Materials* **2007**, *6*, 810.
- Sun, D. M.; Timmermans, M. Y.; Tian, Y.; Nasibulin, A. G.; Kauppinen, E. I.; Kishimoto, S.; Mizutani, T.; Ohno, Y. *Nat Nanotechnol* **2011**, *6*, 156.
- Sangwan, V. K.; Ortiz, R. P.; Alaboson, J. M. P.; Emery, J. D.; Bedzyk, M. J.; Lauhon, L. J.; Marks, T. J.; Hersam, M. C. *ACS Nano* **2012**, *6*, 7480.
- Javey, A.; Guo, J.; Wang, Q.; Lundstrom, M.; Dai, H. *Letters to Nature* **2003**, *424*, 654.
- Kang, S. J.; Kocabas, C.; Ozel, T.; Shim, M.; Pimparkar, N.; Alam, M. A.; Rotkin, S. V.; Rogers, J. A. *Nat Nanotechnol* **2007**, *2*, 230.
- Ryu, K.; Badmaev, A.; Wang, C.; Lin, A.; Patil, N.; Gomez, L.; Kumar, A.; Mitra, S.; Wong, H. S. P.; Zhou, C. W. *Nano Lett.* **2009**, *9*, 189.
- Li, X.; Zhang, L.; Wang, X.; Shimoyama, I.; Sun, X.; Seo, W.-S.; Dai, H. *J. Am. Chem. Soc.* **2007**, *129*, 4890.
- Cao, Q.; Han, S. J.; Tulevski, G. S.; Zhu, Y.; Lu, D. D.; Haensch, W. *Nat Nanotechnol* **2013**, *8*, 180.
- Shekhar, S.; Stokes, P.; Khondaker, S. I. *ACS Nano* **2011**, *5*, 1739.
- Shastry, T. A.; Seo, J. W. T.; Lopez, J. J.; Arnold, H. N.; Kelter, J. Z.; Sangwan, V. K.; Lauhon, L. J.; Marks, T. J.; Hersam, M. C. *Small* **2013**, *9*, 45.
- Engel, M.; Small, J. P.; Steiner, M.; Freitag, M.; Green, A. A.; Hersam, M. S.; Avouris, P. *ACS Nano* **2008**, *2*, 2445.
- Joo, Y.; Brady, G. J.; Arnold, M. S.; Gopalan, P. *Langmuir: the ACS journal of surfaces and colloids* **2014**, *30*, 3460.
- Brady, G. J.; Joo, Y.; Singha Roy, S.; Gopalan, P.; Arnold, M. S. *Appl. Phys. Lett.* **2014**, *104*, 083107.
- Wu, J.; Jiao, L.; Antaris, A.; Choi, C. L.; Xie, L.; Wu, Y.; Diao, S.; Chen, C.; Chen, Y.; Dai, H. *Small* **2013**, n/a.
- King, B.; Panchapakesan, B. *Nanotechnology* **2014**, *25*, 14.
- Kim, B.; Jang, S.; Prabhuramirashi, P. L.; Geier, M. L.; Hersam, M. C.; Dodabalapur, A. *Appl. Phys. Lett.* **2013**, *103*, 082119.
- Miyata, Y.; Shiozawa, K.; Asada, Y.; Ohno, Y.; Kitauro, R.; Mizutani, T.; Shinohara, H. *Nano Research* **2011**, *4*, 963.
- Jin, S. H.; Dunham, S. N.; Song, J.; Xie, X.; Kim, J. H.; Lu, C.; Islam, A.; Du, F.; Kim, J.; Felts, J.; Li, Y.; Xiong, F.; Wahab, M. A.; Menon, M.; Cho, E.; Grosse, K. L.; Lee, D. J.; Chung, H. U.; Pop, E.; Alam, M. A.; King, W. P.; Huang, Y.; Rogers, J. A. *Nat Nanotechnol* **2013**, *8*, 347.
- Iijima, S.; Brabec, C.; Maiti, a.; Bernholc, J. *J. Chem. Phys.* **1996**, *104*, 2089.
- Someya, T.; Sekitani, T.; Iba, S.; Kato, Y.; Kawaguchi, H.; Sakurai, T. *Proc. Natl. Acad. Sci. U.S.A.* **2004**, *101*, 9966.
- Cao, Q.; Kim, H.-s.; Pimparkar, N.; Kulkarni, J. P.; Wang, C.; Shim, M.; Roy, K.; Alam, M. a.; Rogers, J. a. *Nature* **2008**, *454*, 495.
- Zhou, L.; Wanga, A.; Wu, S. C.; Sun, J.; Park, S.; Jackson, T. N. *Appl. Phys. Lett.* **2006**, *88*, 0.
- Xu, F.; Wu, M. Y.; Safron, N. S.; Roy, S. S.; Jacobberger, R. M.; Bindl, D. J.; Seo, J. H.; Chang, T. H.; Ma, Z. Q.; Arnold, M. S. *Nano Lett.* **2014**, *14*, 682.
- Perebeinos, V.; Avouris, P. *Nano Lett.* **2007**, *7*, 609.
- Bindl, D. J.; Safron, N. S.; Arnold, M. S. *ACS Nano* **2010**, *4*, 5657.
- Bindl, D. J.; Wu, M. Y.; Prehn, F. C.; Arnold, M. S. *Nano Lett.* **2011**, *11*, 455.
- Bindl, D. J.; Wu, M.-Y.; Prehn, F. C.; Arnold, M. S. *Nano Lett.* **2011**, *11*, 455.
- Wu, M.-Y.; Jacobberger, R. M.; Arnold, M. S. *J. Appl. Phys.* **2013**, *113*.
- Bindl, D. J.; Arnold, M. S. *J. Phys. Chem. C* **2013**, *117*, 2390.
- Shea, M. J.; Arnold, M. S. *Appl. Phys. Lett.* **2013**, *102*, 5.
- Wu, M. Y.; Jacobberger, R. M.; Arnold, M. S. *J. Appl. Phys.* **2013**, *113*, 15.
- Ye, Y.; Bindl, D. J.; Jacobberger, R. M.; Wu, M.-Y.; Roy, S. S.; Arnold, M. S. *Small* **2014**, n/a.
- Gong, M.; Shastry, T. A.; Xie, Y.; Bernardi, M.; Jasion, D.; Luck, K. A.; Marks, T. J.; Grossman, J. C.; Ren, S.; Hersam, M. C. *Nano Lett.* **2014**, *14*, 5308.
- Ramuz, M. P.; Vosgueritchian, M.; Wei, P.; Wang, C.; Gao, Y.; Wu, Y.; Chen, Y.; Bao, Z. *ACS Nano* **2012**, *6*, 10384.
- Nanot, S.; Cummings, A. W.; Pint, C. L.; Ikeuchi, A.; Akiho, T.; Sueoka, K.; Hauge, R. H.; Leonard, F.; Kono, J. *Scientific Reports* **2013**, *3*.

## Carbon Nanotubes

For a complete list of available materials, visit [aldrich.com/cnt](http://aldrich.com/cnt).

### Single-walled Carbon Nanotubes

Production Method	Dimensions	Purity	Prod. No.
CoMoCAT® Catalytic Chemical Vapor Deposition (CVD) Method (6,5) chirality	diameter 0.7 - 0.9 nm (by fluorescence)	≥93% (carbon as SWNT)	<a href="#">773735-250MG</a> <a href="#">773735-1G</a>
	diameter 0.7 - 0.9 nm (by fluorescence) L ≥700 nm	≥77% (carbon as SWNT)	<a href="#">704148-250MG</a> <a href="#">704148-1G</a>
CoMoCAT® Catalytic Chemical Vapor Deposition (CVD) Method (7,6) chirality	diameter 0.7 - 1.1 nm L 300-2300 nm (mode: 800nm; AFM)	≥77% (carbon as SWNT)	<a href="#">704121-250MG</a> <a href="#">704121-1G</a>
	CoMoCAT® Catalytic Chemical Vapor Deposition (CVD) Method	diameter 0.6 - 1.1 nm	>95% (carbon as SWCNT)
diameter 0.7 - 1.4 nm		≥80.0% (carbon as SWNT)	<a href="#">724777-250MG</a> <a href="#">724777-1G</a>
diameter 0.7 - 1.3 nm L 450-2300 nm (mode: 800nm; AFM)		≥70% (carbon as SWNT)	<a href="#">704113-250MG</a> <a href="#">704113-1G</a>

## Single-walled Carbon Nanotube (cont'd)

Production Method	Dimensions	Purity	Prod. No.
Catalytic Carbon Vapor Deposition (CCVD) Method	average diameter 2 nm × L × 3 (TEM)	>70%	755710-250MG 755710-1G
Electric Arc Discharge Method	diameter 1.2 - 1.7 nm L 0.3-5 μm	30% (Metallic) 70% (Semiconducting)	750492-100MG
	diameter 1.2 - 1.7 nm L 0.3-5 μm	30% (Metallic) 70% (Semiconducting)	750514-25MG
	diameter 1.2 - 1.7 nm L 0.3-5 μm	2% (Metallic) 98% (Semiconducting)	750522-1MG
	diameter 1.2 - 1.7 nm L 0.3-5 μm	98% (Metallic) 2% (Semiconducting)	750530-1MG
	D × L 2-10 nm × 1-5 μm (bundle dimensions) 1.3-1.5 nm (individual SWNT diameter)	40-60 wt. %	698695-1G 698695-5G

## Single-walled Carbon Nanotube Inks

Form	SWCNT Concentration	Viscosity	Sheet Resistance	Prod. No.
dispersion in H <sub>2</sub> O (black liquid)	0.20 +/- 0.01 g/L (by Absorbance at 854 nm)	~1.0 mPa.s	<400 Ω/sq (by 4-point probe on prepared film by spray)	791490-25ML 791490-100ML
	1.00 +/- 0.05 g/L (SWCNT concentration by Absorbance at 854 nm)	3.0 mPa.s (at 10 sec <sup>-1</sup> shear rate)	<600 Ω/sq (at 85% VLT (ohm/square), by 4-point probe on prepared film by spray)	791504-25ML 791504-100ML
viscous liquid (black)	1 mg/mL	17.7 Pa.s at 25 °C (at 10 sec <sup>-1</sup> shear rate)	<1000 Ω/sq (by 4-point probe on prepared, at 87.5% VLT (ohm/sq))	792462-25ML 792462-100ML

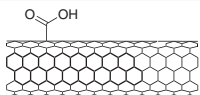
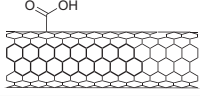
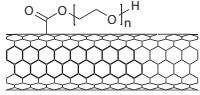
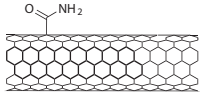
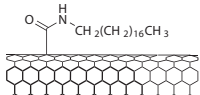
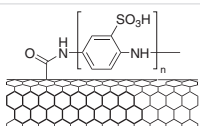
## Double-walled Carbon Nanotubes

Production Method	Dimensions	Purity	Prod. No.
Catalytic Carbon Vapor Deposition (CCVD) Method	avg. diam. × L 3.5 nm × >3 μm (TEM)	Metal Oxide ≤10% TGA	755141-1G
	avg. diam. × L 3.5 nm × 1-10 μm (TEM)	Metal Oxide <10% TGA	755168-1G
Chemical Vapor Deposition (CVD) Method	O.D. × I.D. × L 5 nm × 1.3-2.0 nm × 50 μm	50-80%	637351-250MG 637351-1G

## Multi-walled Carbon Nanotubes

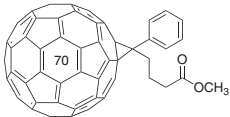
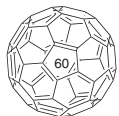
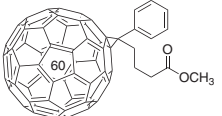
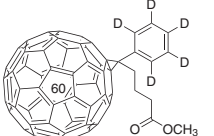
Production Method	Description	Purity	Prod. No.
CoMoCAT <sup>®</sup> Catalytic Chemical Vapor Deposition (CVD) Method	O.D. × I.D. × L 10 nm ±1 nm × 4.5 nm ±0.5 nm × 3--6 μm (TEM)	≥98% carbon basis	773840-25G 773840-100G
	O.D. × L 6-9 nm × 5 μm diam. 6.6 nm (median) diam. 5.5 nm (mode)	>95% (carbon)	724769-25G 724769-100G
	O.D. × I.D. × L 10 nm × 4.5 nm × 4 μm Aspect ratio (L/D) 350-550 Tubes typically have 6-8 tube walls.	70-80% (carbon)	791431-25G 791431-100G
	Catalytic Carbon Vapor Deposition (CCVD) Method	avg. diam. × L 9.5 nm × <1 μm (TEM) thin and short	Metal Oxide <5% TGA
Chemical Vapor Deposition (CVD) Method	avg. diam. × L 9.5 nm × 1.5 μm (TEM) thin	Metal Oxide <5% TGA	755133-5G
	O.D. × L 6-13 nm × 2.5-20 μm 12 nm (average diameter, HRTEM) 10 μm (average length, TEM)	>98% carbon basis	698849-1G
	D × L 110-170 nm × 5-9 μm	>90% carbon basis	659258-2G 659258-10G
Electric Arc Discharge Method	O.D. × L 7-12 nm × 0.5-10 μm powdered cylinder cores	20-30% MWCNT basis	406074-500MG 406074-1G 406074-5G
	O.D. × L 7-15 nm × 0.5-10 μm as-produced cathode deposit	>7.5% MWCNT basis	412988-100MG 412988-2G 412988-10G
Plasma-Enhanced Chemical Vapor Deposition (PECVD) Method	diam. × L 100-150 nm × 30 μm (SEM) vertically aligned on silicon wafer substrate	>95 atom % carbon basis(x-ray)	687804-1EA

## Functionalized Nanotubes

Structure	Name	Purity (%)	Dimensions	Production Method	Prod. No.
	Carbon nanotube, single-walled, carboxylic acid functionalized	>90	D × L 4-5 nm × 0.5-1.5 μm (bundle dimensions)	Electric Arc Discharge Method	<a href="#">652490-250MG</a> <a href="#">652490-1G</a>
	Carbon nanotube, multi-walled, carboxylic acid functionalized	>80	avg. diam. × L 9.5 nm × 1.5 μm	Catalytic Carbon Vapor Deposition (CCVD) Method	<a href="#">755125-1G</a>
	Carbon nanotube, single-walled, poly(ethylene glycol) functionalized	>80	D × L 4-5 nm × 0.5-0.6 μm (bundle dimensions)	Electric Arc Discharge Method	<a href="#">652474-100MG</a>
	Carbon nanotube, single-walled, amide functionalized	>90	D × L 4-6 nm × 0.7-1.0 μm (bundle dimensions)	Electric Arc Discharge Method	<a href="#">685380-100MG</a>
	Carbon nanotube, single-walled, octadecylamine functionalized	80-90	D × L 2-10 nm × 0.5-2 μm (bundle dimensions)	Electric Arc Discharge Method	<a href="#">652482-100MG</a>
	Carbon nanotube, single-walled, polyaminobenzene sulfonic acid functionalized	75-85	D × L 1.1 nm × 0.5-1.0 μm (bundle dimensions)	Electric Arc Discharge Method	<a href="#">639230-100MG</a>

## Fullerenes

For a complete list of available materials, visit [aldrich.com/fullerene](http://aldrich.com/fullerene).

Structure	Name	Purity (%)	Prod. No.
	[5,6]-Fullerene-C <sub>70</sub>	≥99	<a href="#">709476-250MG</a>
		98	<a href="#">482994-100MG</a> <a href="#">482994-500MG</a>
	[6,6]-Phenyl C <sub>71</sub> butyric acid methyl ester, mixture of isomers	99	<a href="#">684465-100MG</a> <a href="#">684465-500MG</a>
	Fullerene-C <sub>60</sub>	99.9	<a href="#">572500-250MG</a> <a href="#">572500-1G</a> <a href="#">572500-5G</a>
		99.5	<a href="#">379646-1G</a> <a href="#">379646-5G</a>
		98	<a href="#">483036-1G</a> <a href="#">483036-5G</a>
	[6,6]-Phenyl C <sub>61</sub> butyric acid methyl ester	>99.9	<a href="#">684457-100MG</a>
		>99.5	<a href="#">684449-100MG</a> <a href="#">684449-500MG</a>
		>99	<a href="#">684430-1G</a>
	[6,6]-Pentadeuterophenyl C <sub>61</sub> butyric acid methyl ester	99.5	<a href="#">684503-100MG</a>

## Fullerenes (cont'd)

Structure	Name	Purity (%)	Prod. No.
	[6,6] Diphenyl C <sub>60</sub> bis(butyric acid methyl ester)(mixture of isomers)	99.5	704326-100MG
	[6,6]-Phenyl-C <sub>61</sub> butyric acid butyl ester	>97	685321-100MG 685321-1G
	[6,6]-Phenyl-C <sub>61</sub> butyric acid octyl ester	≥99	684481-100MG
	[6,6]-Thienyl C <sub>61</sub> butyric acid methyl ester	≥99	688215-100MG
	N-Methylfulleropyrrolidine	99	668184-100MG
	Small gap fullerene-ethyl nipecotate	≥95, fullerenes 50%	707473-250MG
	ICMA	97	753947-250MG
	ICBA	99	753955-250MG
	Polyhydroxy small gap fullerenes, hydrated	Polyhydroxy SGFs(TGA) ~ 85%	707481-100MG
	Polyhydroxylated fullerenes, water soluble	-	793248-100MG

# NOVEL GRAPHENE-BASED NANOSTRUCTURES PRODUCTION, FUNCTIONALIZATION, AND ENGINEERING



Manuela Melucci,<sup>1</sup> Simone Ligi,<sup>2</sup> Vincenzo Palermo<sup>3\*</sup>  
<sup>1</sup>ISOF – Consiglio Nazionale delle Ricerche (CNR), Italy  
<sup>2</sup>GNext sas, Italy  
<sup>3</sup>ISOF – Consiglio Nazionale delle Ricerche (CNR), Italy  
 \*Email: vincenzo.palermo@isof.cnr.it

## Introduction

At the beginning of its exciting life, graphene was mostly a game for physicists. Due to the difficulty of producing sufficient amounts of high-quality graphene, researchers used single sheets of graphene exfoliated with adhesive tape in very simple geometries to study the outstanding electronic properties of this new material. Ten years after the initial revolution, graphene has gained enormous attention among the general public, being the most “followed” material in online social media and commonly considered as the new wonder material.<sup>1</sup>

However, major issues hindering the wide application of graphene are still present, including poor processability, and for electronics, the lack of a bandgap in its electronic structure.

More recently, chemists have learned how to “play” with this unique material by enhancing its processability and versatility, and developing different strategies to functionalize and process it. The production of graphene starting from cheap graphite has been demonstrated on a large scale,<sup>2</sup> growth of high quality graphene on metallic substrates or on silicon carbide has been optimized, and applications in different fields have been demonstrated at commercial or prototype level.<sup>3,4</sup>

Our previous works described how the peculiar two-dimensional (2D) shape of graphene gives it unique properties<sup>5</sup> such as its interaction with organic molecules in vacuums, liquids, and solid films.<sup>6</sup>

Using chemistry, it is possible to effectively tailor this poorly soluble and almost chemically inert material into a wide variety of forms ranging from simple, soluble sheets to hierarchical architectures where 2D graphene sheets are assembled into three-dimensional (3D) bulk materials or foams for applications in electronics, composites, energy storage, or catalysis.

## Graphene Chemistry in Solution at Single-sheet Level

The simplest way to process and tailor graphene is to work with single sheets in solution. Production on a large scale can be achieved either using “soft” approaches, i.e., non-covalent supramolecular interactions that do not damage the graphene lattice,<sup>7–9</sup> or “harsh” chemical approaches, i.e., oxidation to graphene oxide (GO) and subsequent reduction that inevitably results in chemical defects on the surface of the sheets (Figure 1).<sup>10–12</sup>

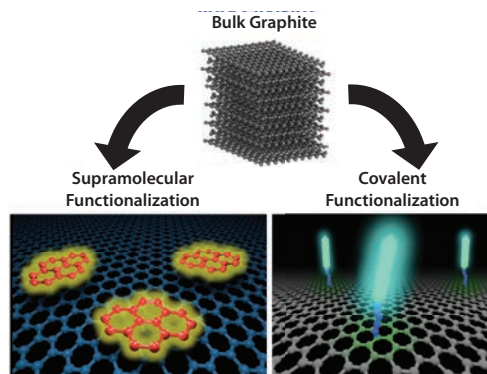


Figure 1. Schematic of different approaches to exfoliate graphite and functionalize graphene by using covalent or non-covalent (supramolecular) approaches.

GOs (Aldrich Prod. Nos. **763705**, **777676**, **794341**, etc.) have long been the underdog of the graphene family due to their chemical defects that diminish many of the unique physical properties of graphene. However, these same characteristics make GOs highly processable, versatile, and water soluble. Thermal, chemical, or electrochemical reduction can be used to re-establish conductivity, but some damage to the lattice always remains, giving reduced graphene oxide (RGO) (Aldrich Prod. No. **777684**) much less performance than graphene. Nevertheless, production and successful application of different forms of GO and RGO have been demonstrated;<sup>13–20</sup> some of them seem even closer to commercial applications than the most advertised applications of graphene for electronics or transparent conductors.

The exfoliation of graphite (Aldrich Prod. Nos. **496588**, **496596**, etc.) to produce graphene is a complex phenomenon that takes place on a nano- and mesoscopic scale. Similar to other solubilization processes, the process depends on a complex competition between chemical, electrostatic, and Van der Waals interactions,<sup>21</sup> as well as on fluid dynamics

at the micro-scale. Recently, we conducted a systematic and comparative study on exfoliated graphene produced using mechanical, chemical, and electrochemical approaches.<sup>22</sup> Among the three methods, chemical oxidation to produce GO was found to be a very effective but disruptive method to exfoliate graphite. Electrochemical oxidation, which uses electric fields to drive molecular intercalation in graphite, allows for a fast exfoliation and in-depth disruption of bulk quantities of graphite, but also results in damage to the resulting graphene lattice.

The supramolecular exfoliation approach, based on sonication in organic solvents, yields graphene of the best quality, but due to the high-energy input requirements of the sonication process, sheets with low lateral size (typically <1 μm) are obtained. The differences observed from the three methods demonstrate the existing trade-off between speed and efficiency of exfoliation on one side, and preservation of material quality on the other.<sup>22</sup>

Once exfoliated in solution, graphene sheets can be chemically modified (both covalently and non-covalently) using a variety of molecules or nano-objects to yield new, property-specific, tailored, graphene-based materials.<sup>23</sup> The highly conjugated sp<sup>2</sup> carbon structure of graphene gives it a strong affinity to polyaromatic organic materials, such as organic semiconductors or industrial dyes characterized by extended π-electrons delocalization. These molecules, unlike graphene, have excellent processability and tunable HOMO, LUMO, and bandgap.<sup>6</sup>

This affinity is currently being investigated in order to create graphene-organic hybrids with enhanced solubility in water or organic solvents, good dispersibility in polymer composites and/or novel optoelectronic functions. Although it is difficult to give a fair and exhaustive overview on all the graphene-based hybrid systems developed so far, interesting examples include hybrids based on organic materials, as well as metal nanoparticles and biomolecules, even DNA. Most common moieties used are perylenes (Aldrich Prod. No. 394475, etc.),<sup>9,24,25</sup> pyrenes (Aldrich Prod. No. 571245, etc.),<sup>8,26-29</sup> porphyrins (Aldrich Prod. No. 252921, etc.),<sup>30-34</sup> fullerenes (Aldrich Prod. No. 572500, etc.),<sup>35</sup> oligothiophenes (Aldrich Prod. No. 691631, etc.),<sup>36,37</sup> polythiophenes (Aldrich Prod. No. 698997, etc.),<sup>38,39</sup> metal nanoparticles,<sup>40,41</sup> or even biological moieties.<sup>42,43</sup>

There are several empirical models that use the surface tension of the solvent or solubility parameters to predict the dispersion of graphene in different solvents.<sup>7</sup> However, there is still no clear understanding at the molecular level why some molecules interact with graphene more effectively than others. We conducted a systematic study to compare the efficiency of several pyrenesulfonic acid sodium salts (Sigma Prod. Nos. 82657, 37920 and 82658, and Aldrich Prod. No. H1529), the water-soluble pyrene moieties, as exfoliation agents for the preparation of stable aqueous suspensions using liquid exfoliation.<sup>8</sup> These pH-sensitive derivatives are not only interesting for fundamental research, but also for practical applications due to their high photoluminescence quantum yield, excellent water solubility, and lack of toxicity. They also have large-scale, commercial applications in highlighters, pencils, and soaps.

We examined a series of four pyrene derivatives featuring an increasing number of polar groups and found all of them exfoliate graphite, yielding stable suspensions of graphene in water. A relevant fraction of monolayer graphene sheets covered by a layer of pyrene molecules was obtained.<sup>26</sup> The total concentration of suspended graphene depends significantly on the number of polar groups on the hydrophobic pyrene core. Molecular dynamic calculations revealed that a critical factor in the interaction of pyrene derivatives with graphene involves a thin layer of solvent molecules, confined between the pyrene molecules and the graphene surface. The amphiphilic pyrenesulfonic molecule changes its orientation when approaching the surface to slide into this layer in a most effective way for molecules with an asymmetric shape showing a strong dipole. Simulations indicate the molecular dipole is not important per se, but

it facilitates the “sliding” of the molecule into the solvent layer, resulting in the lateral displacement of the water molecules located between the aromatic core of the pyrene dye and the graphene substrate.

The interaction of organic molecules on graphene sheets at the nanoscale is not only of great interest from the fundamental point of view to better understand and improve graphene exfoliation,<sup>8</sup> but also has important implications for advanced applications. Thus, the pyrene-based method to exfoliate graphite with a well-established industrial dye was extended to process graphene in polymers.<sup>45</sup> The same pyrenesulfonic acids have shown a similar ability to solubilize other 2D materials such as boron nitride (Aldrich Prod. Nos. 255475 and 790532), tungsten disulfide (Aldrich Prod. Nos. 243639 and 790583), molybdenum disulfide (Aldrich Prod. Nos. 234842 and 69860), selenides, and tellurides (Figure 2). The materials can be used to fabricate a photodetector device based on different layers of 2D materials.<sup>44</sup>

### Processing of 2D Materials with Supramolecular Interactions

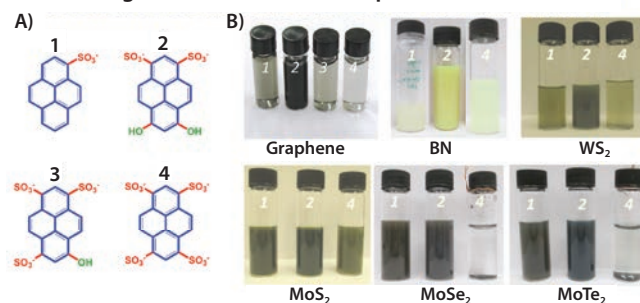


**Figure 2.** A) Chemical formula of four pyrene derivatives compared for supramolecular graphite exfoliation. B) Optical images of the as-prepared 2D crystal-based dispersions using pyrene derivatives (the numbers 1, 2, 3 and 4 refer to the number of sulphonic groups of the organic dyes shown in A).<sup>8,44</sup>

In parallel to non-covalent modification approaches based on supramolecular interactions, different synthetic methods have been proposed worldwide to covalently bind functional organic materials onto graphene and graphene oxide. The development of more efficient and controlled synthetic protocols to achieve this aim is a challenging issue. Given the poor dispersibility and intrinsic inert chemical structure of graphene, its reactivity is much more limited than that of GO, and most mainly rely upon the formation of covalent bonds between free radicals or dienophiles and C=C bonds.<sup>46,47</sup> Conversely, GO can undergo the reactions typical of carboxylic, carbonyl, epoxide, and hydroxyl functionalities; thus, it is easier to modify than graphene. Among the most common synthetic methods for GO functionalization is the activation of the carboxylic moieties followed by reaction with nucleophilic groups (i.e., amines<sup>37</sup>). One recent proposed alternative for GO functionalization relies on silylation of surface oxydrilic groups promoted by MW irradiation. This method can be used to graft trialkoxysilane ended π-conjugated chromophores on GO sheets surface.<sup>36</sup>

Several authors have studied how the properties of functional molecular materials influence the behavior of graphene after physical doping<sup>48-50</sup> or covalent engrafting.<sup>37,51</sup> At the same time, the question of how the properties of the molecule will be affected by the presence of graphene remains. It is well-known that graphene and GO strongly quench the photoemission of light-emitting molecules,<sup>52-54</sup> but how much is this interaction influenced by the nanoscale structure of this graphene-organic ensemble? By engineering the structure of the system at the nanoscale, it is possible to tune this interaction. For example, low quenching (~16%) is observed when oligothiophene dyes are tethered to GO using flexible alkyl linkers,<sup>37</sup> stronger quenching (~60%) is achieved with shorter linkers,<sup>51</sup> and nearly complete quenching

is attained by depositing GO on a self-assembled monolayer of the same oligothiophenes (Aldrich Product Nos. 547905 and 594687)<sup>52</sup> (see Figure 3A).

### GO-Organic Covalent Composites

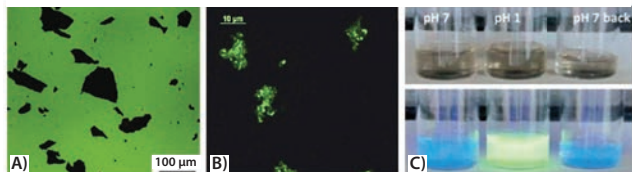


**Figure 3.** A) GO sheets quenching the fluorescence of a thin layer of oligothiophene molecules on SiO<sub>2</sub>.<sup>52</sup> B) Fluorescent GO sheets, obtained by functionalization of GO with oligothiophene dyes, using a flexible diamine linker.<sup>37</sup> C) Images of GO-oligothiophene covalent composites in EtOH at neutral pH, upon acidification with HCl and re-neutralization by triethylamine (TEA) (from left to right) under normal light (top) and UV irradiation (bottom) showing the reversible emission switch.<sup>37</sup>

Besides fluorescence quenching, the same oligothiophene-GO ensemble was used to study how tethering the molecule to GO affects its chemophysical properties. Molecules will behave differently when isolated in a solvent rather than tethered to a bulk, macroscopic surface. However, molecules tethered to graphene or GO are in an ambiguous situation since the size of a 2D sheet is much larger than that of a typical molecule. This is, in fact, more comparable to attachment to a bulk conventional surface but simultaneously dissolved in solution.<sup>5</sup> We examined the interaction of GO with a terthiophene dye using pH-sensitive fluorescence emission to determine how the emission changes when the molecules are free in solution or tethered to a GO (Figures 3B–C). We found that covalent attachment to GO does not perturb the absorption and emission properties of the dye and, in particular, the pH sensitivity.

## From Solution to Real Materials

Once the 2D sheets of graphene (or chemically modified graphene) have been processed and functionalized in solution (either by exploiting supramolecular interactions or by passing through graphene oxide), it is very easy to deposit them on silicon substrates with micro/nano electrodes to create devices such as transistors or sensors. Taking advantage of the high processability and easy charge transfer between graphene and organic materials, it is possible to prepare devices with tunable percolation that allow it to merge the good charge mobility of RGO with the semiconducting behavior of organic materials.

Some recently published examples include RGO/poly(3-hexylthiophene) bilayers,<sup>18</sup> graphene/phenyloctane, and graphene/arachidic acids blends;<sup>55</sup> and graphene blends with high-performing semiconductive polymers, like poly[N,N-9-bis(2-octylododecyl)-naphthalene-1,4,5,8-bis(dicarboximide)-2,6-diy]-alt-5,59-(2,29-bithiophene)], and (P(NDI2OD-T2)).<sup>56</sup>

The graphene and the organics can be deposited simultaneously to form a thick intermixed blend,<sup>55,56</sup> or sequentially to form a bilayer.<sup>18</sup>

Utilizing the ability of organic  $\pi$ -conjugated molecules to exfoliate graphite,<sup>8,55</sup> graphene exfoliation can be performed in the same solution used for the organic material deposition on devices. Alternatively, an *ex situ* two-stage approach based on more “classical” solvents to exfoliate graphite and subsequent mixing with the organic semiconductor can be used.<sup>56</sup> By using the suitable solvents and applying electric fields, it is possible to deposit the sheets selectively on the source, the drain, or in between the electrodes.<sup>57,58</sup>

## Processing Graphene in More Complex, Multilayer Structures

In addition to simple mixtures or bilayers with semiconducting polymers, more complex structures can be constructed by taking advantage of the enhanced processability and tunability of chemically modified graphene.

Multilayer “sandwich” structures can be engineered using high-quality graphene alternated to self-assembled monolayers of 1-pyrenebutyric acid N-hydroxysuccinimide using layer-by-layer (LbL) deposition. Such multilayered structures showed an enhancement of six orders of magnitude in electric conductivity, as compared to pure graphene, due to graphene doping by pyrene.<sup>59</sup>

In a similar approach, multilayer structures of GO alternated to poly-L-lysine can be created using LbL. Heating to 800 °C, the GO is reduced and doped with poly-lysine, yielding micro-supercapacitors with an ultrahigh volumetric capacitance of ~488 F/cm<sup>3</sup> and an outstanding rate capability of up to 2,000 V/s.

GO-based structures with 2D porosity can be obtained using covalent functionalization with linkers of variable length. For example, the *p*-xylylenediamine intercalation reaction of graphene oxide (GO) is a convenient and simple approach to prepare pillared-type graphene-based materials.<sup>60</sup> The generation of such a constrained system (covalently “stitched”) along the graphene *c*-axis allows it to considerably change the interlayer distance when compared to pristine GO, thanks to a cross-linking process of the *p*-xylylenediamine (Aldrich Prod. No. 279633) with the epoxide surface groups of adjacent GO sheets. The increased GO interlayer distance provides materials with increased porosity and specific surface areas up to five times higher than those of pristine GO.

A more coarse-grained structure has been obtained creating multilayers of solvent-exfoliated graphene sheets and thin layers of vacuum-sublimed metallic tin. Upon annealing at 300 °C in Ar/H<sub>2</sub>, the tin layer breaks down into isolated nanopillars that act as spacers for graphene and as an ion reservoir for lithium storage in batteries (Figure 4A).<sup>61</sup>

The as-formed 3D multilayered nanostructure was directly used as an anode material for rechargeable lithium-ion batteries without adding any polymer binder or carbon black. Electrochemical measurements showed very high reversible capacity and excellent cycling performance at a current density as high as 5 A g<sup>-1</sup>. This is a good example of how novel structures can be obtained by combining liquid processing with vacuum-based techniques such as thermal evaporation.

In another example, highly uniform sandwiches of GO sheets embedded in porous carbon (PC) were obtained using ionic liquid functionalized graphene-oxide sheets as a shape-directing agent and a resorcinol/formaldehyde polymer as the carbon precursor. The PC/GO/PC multilayer sandwich structures obtained show excellent rate capability, a high specific capacitance of 341 F g<sup>-1</sup> at 5 mV s<sup>-1</sup>, and good cycle stability over 35,000 cycles without any conductive additive.

The production of graphene composites at single-sheet level in solution or in very thin layers on flat substrates, has been described mostly for electronics applications. Moving to an even larger scale, more complex structures can be constructed by using mesoscopic templates to obtain bulk, macroscopic hierarchical materials.

## Increasing Complexity Up To the Macroscale: Foams for Energy Storage or Catalysis

By experimenting with the oxidation, reduction, and/or chemical functionalization of GO, 2D sheets of different kinds can be processed or even directly grown on virtually any micro- or nano-porous templates like metallic<sup>62,63</sup> or polymeric foams,<sup>64</sup> inorganic ZnO nanocrystals,<sup>65</sup> or water-organic liquid interfaces in emulsions.<sup>66,67</sup> Graphene can be used to wrap or coat other nanostructures<sup>68</sup> or even electrodes.<sup>58</sup> Conversely, its surface can be coated with other materials acting as a 2D substrate to support less conductive or less robust materials.<sup>69,71</sup>

These architectures are often visually beautiful (Figures 4–5), but also interesting from the technological point of view because they can be further functionalized with other materials having properties synergistic and complementary to those of graphene.

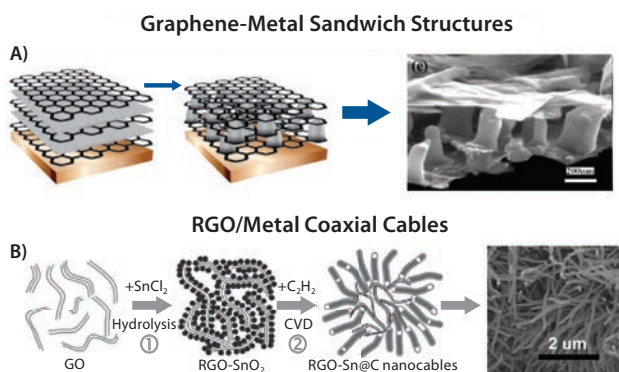


**Figure 4.** A) Schematic of the graphene/Sn-nanopillar nanostructure preparation procedures, and corresponding SEM image.<sup>61</sup> B) Schematic of procedures for the synthesis of RGO-supported Sn/C nanocables, and corresponding SEM image.<sup>71</sup>

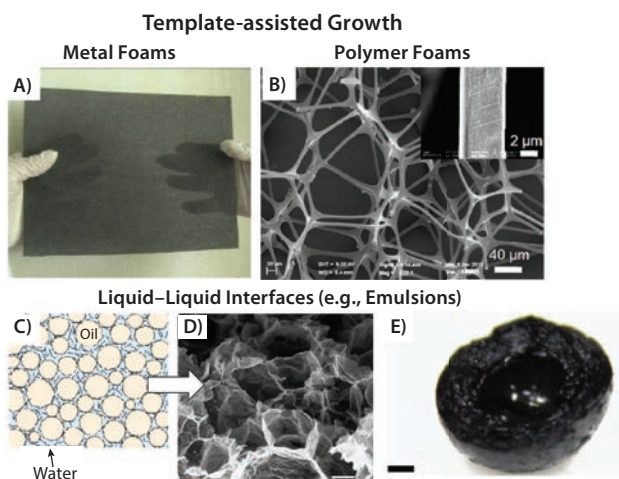


**Figure 5.** Graphene-based 3D structures templated using A) metal foams,<sup>62</sup> B) polymeric foams,<sup>64</sup> or C–E) in liquid emulsions.<sup>66</sup>

Graphene has outstanding electrical, optical, mechanical, and thermal properties, but contrary to the media hype, it can't be good at everything. Some other materials have better properties for energy applications;  $\text{Fe}_2\text{O}_3$  is a promising low-cost, abundant, and non-toxic candidate for pseudo-capacitor electrodes with high theoretical capacity ( $1,007 \text{ mA h g}^{-1}$ ), much better than that of commonly used graphite-based materials ( $372 \text{ mA h g}^{-1}$ ). However, the practical applications of  $\text{Fe}_2\text{O}_3$ -based electrodes are limited due to their low electrical conductivity and inferior

cycling stability. Thus, the combination of graphene and  $\text{Fe}_2\text{O}_3$  is of high interest for the development of next-generation batteries.

We produced hierarchical graphene-based composites with  $\text{Fe}_2\text{O}_3$  for energy storage using a combination of electrochemical and solution-processing techniques. Electrochemically exfoliated graphene oxide (EGO) sheets were produced using a custom-built setup that allowed fast expansion of graphite flakes and efficient exfoliation of expanded graphite via an electrochemical route. The resulting sheets were deposited on sacrificial nickel foam together with an iron hydroxide colloidal precursor. Subsequent calcination treatment simultaneously rendered the EGO foam conductive and transformed  $\text{Fe}(\text{OH})_3$  into hematite ( $\alpha\text{-Fe}_2\text{O}_3$ ), yielding a nanoporous  $\text{Fe}_2\text{O}_3$  layer on the surface of the mesoporous EGO foam. The resulting graphene/metal oxide hybrid was a continuous, electrically conductive 3D composite, that made an ideal structure for lithium storage (Figure 6), featuring a hierarchical meso-nano porous structure (Figures 7A–D). By using liquid processing, the nanostructured material can be optimized by tuning the  $\text{Fe}_2\text{O}_3$ :EGO ratio in order to maximize performance as standard coin cell battery electrodes.<sup>63</sup>

With the decoration of  $\text{Fe}_2\text{O}_3$  nanoporous coatings, the initial discharge capacities can be enhanced up to  $701 \text{ mA h g}^{-1}$ , a value comparable to commercially available batteries, and a higher energy capacity can be retained after the first discharge/charge cycle (Figure 7E).

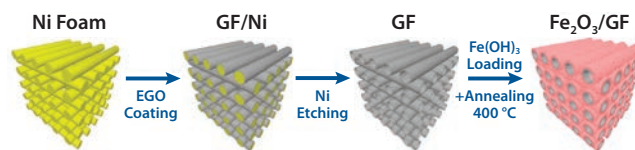


**Figure 6.** Schematic of template-assisted deposition of electrochemically exfoliated graphene oxide (EGO) on a nickel metallic foam, and successive reduction to give conductive foams (GF), either uncoated or coated with iron oxide (hematite).<sup>63</sup>

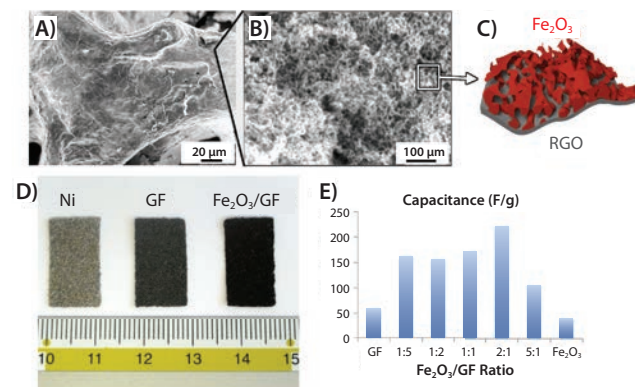


**Figure 7.** A) SEM image of a mesoporous, conductive graphene foam coated with a nanoporous layer of iron oxide. B) Inset of A). C) Illustration showing the hierarchical structure of the  $\text{Fe}_2\text{O}_3$ /GF porous layer. D) Photograph comparing the original Ni foam, the GF and the  $\text{Fe}_2\text{O}_3$ /GF samples. E) Specific capacitance values obtained varying  $\text{Fe}_2\text{O}_3$ :GF ratio.<sup>63</sup>

In addition to energy storage, catalysis is another promising field where graphene-based porous structures can be used. In particular, graphene-based materials have shown promise as efficient cathode catalysts for the oxygen reduction reaction (ORR), a critical process in fuel cells.

$\text{Fe}_2\text{O}_3$ /graphene foams show a more positive onset potential, higher cathodic density, and higher electron transfer numbers for the ORR in alkaline media than  $\text{Fe}_3\text{O}_4$  nanoparticles supported on more conventional materials (N-doped carbon black or N-doped graphene sheets). This improvement can be attributed to the role of the 3D macropores and the high specific surface area of the graphene-based support for improving the ORR performance.<sup>69</sup> A more detailed review on the use of porous graphene materials for advanced electrochemical energy storage and conversion can be found in Reference 72.

## Conclusions

The field of graphene chemical exfoliation, processing, and functionalization is currently bursting with several scientific results being published every month. It is expected this trend will accelerate even more in the next years as graphene with standardized quality, well-controlled properties, and low cost becomes more widely available for industrial applications all over the world. Affordable prices are already claimed for powders of multi-layer graphene and applications that use graphene based composites are already available to the end-user market. Moreover, chemical functionalization can enhance the interaction of graphene with polymeric matrices in composites to improve mechanical properties while allowing for the use of very low amounts of graphene.

Even more than its outstanding electronic properties, the chemical versatility and processability of graphene enables production of an exceptionally wide range of materials with advanced and unprecedented functionalities. In fact, the field of chemistry itself is experiencing a graphene-stimulated revival. Conventional organic chemistry methods need to be properly readapted for graphene tailoring, representing a challenging issue for organic chemists. In parallel, novel *ad hoc* protocols and reactions have to be developed for the realization of different composite materials: from simple graphene sheets coated by a thin layer of molecules, to bulk composites of graphene and organic materials, to more complex forms where graphene acts as a 3D, robust, and versatile scaffold to be combined with organic, inorganic, or even biological materials.

## Acknowledgments

The research leading to these results has received funding from the European Union Seventh Framework Programme under grant agreement n°6404391 Graphene Flagship, the EC Marie-Curie ITN- iSwitch (GA no. 642196). The project UPGRADE acknowledges the financial support of the Future and Emerging Technologies (FET) programme within the Seventh Framework Programme for Research of the European Commission, under FET-Open grant number: 309056. We acknowledge the Operative Program FESR 2007-2013 of Regione Emilia-Romagna – Attività I.1.1.

## References

- Sechi, G.; Bedognetti, D.; Sgarrella, F.; Van Eperen, L.; Marincola, F. M.; Bianco, A.; Delogu, L. G. *Nanomedicine* **2014**, *9*, 1475–1486.
- Paton, K. R.; Varrla, E.; Backes, C.; et al. *Nat Mater* **2014**, *13*, 624–630.
- Novoselov, K. S.; Fal'ko, V. I.; Colombo, L.; Gellert, P. R.; Schwab, M. G.; Kim, K. *Nature* **2012**, *490*, 192–200.
- Ferrari, A. C.; Bonaccorso, F.; Falco, V.; et al. *Nanoscale* **2014**, DOI: 10.1039/C1034NR01600A
- Palermo, V.; *Chemical Communications* **2013**, *49*, 2848–2857.
- Schlierf, A.; Samor, P.; Palermo, V. *Journal of Materials Chemistry C* **2014**, *2*, 3129–3143.
- Coleman, J. N. *Accounts of Chemical Research* **2013**, *46*, 14–22.
- Schlierf, A.; Yang, H. F.; Gebremedhn, E.; et al. *Nanoscale* **2013**, *5*, 4205–4216.
- Kozhemyakina, N. V.; Englert, J. M.; Yang, G. A.; Spiecker, E.; Schmidt, C. D.; Hauke, F.; Hirsch, A. *Advanced Materials* **2010**, *22*, 5483–5487.
- Bagri, A.; Mattevi, C.; Acik, M.; Chabal, Y. J.; Chhowalla, M.; Shenoy, V. B. *Nature Chemistry* **2010**, *2*, 581–587.
- Mattevi, C.; Eda, G.; Agnoli, S.; et al. *Adv. Funct. Mater.* **2009**, *19*, 2577–2583.
- Park, S.; Ruoff, R. S. *Nature Nanotechnology* **2009**, *4*, 217–224.
- Panzavolta, S.; Bracci, B.; Gualandri, C.; et al. *Carbon* **2014**, *78*, 566–577.
- Zhao, X.; Xu, Z.; Zheng, B.; Gao, C. *Scientific Reports* **2013**, *3*, #3164.
- Schopp, S.; Thomann, R.; Ratzsch, K.-F.; Kerling, S.; Altstaedt, V.; Muelhaupt, R. *Macromolecular Materials and Engineering* **2014**, *299*, 319–329.
- Borini, S.; White, R.; Wei, D.; Astley, M.; Haque, S.; Spigone, E.; Harris, N.; Kivioja, J.; Ryhänen, T. *ACS Nano* **2013**, *7*, 11166–11173.
- Prezioso, S.; Perrozzi, F.; Giancaterini, L.; Cantalini, C.; Treossi, E.; Palermo, V.; Nardone, M.; Santucci, S.; Ottaviano, L. *Journal of Physical Chemistry C* **2013**, *117*, 10683–10690.
- Liscio, A.; Veronese, G. P.; Treossi, E.; Suriano, F.; Rossella, F.; Bellani, V.; Rizzoli, R.; Samori, P.; Palermo, V. *Journal of Materials Chemistry* **2011**, *21*, 2924–2931.
- S. Rapino, V.; Treossi, E.; Palermo, V.; Marcaccio, M.; Paolucci, F.; Zerbetto, F. *Chemical Communications* **2014**, *50*, 13117–13120.
- Liu, Z.; Parvez, K.; Li, R.; Dong, R.; Feng, X.; Mullen, K. *Advanced materials (Deerfield Beach, Fla.)* **2015**, *27*, 669–675.
- Palermo, V.; Samori, P. *Angewandte Chemie-International Edition* **2007**, *46*, 4428–4432.
- Xia, Z. Y.; Pezzini, S.; Treossi, E.; Giambastiani, G.; Corticelli, F.; Morandi, V.; Zanelli, A.; Bellani, V.; Palermo, V. *Advanced Functional Materials* **2013**, *23*, 4684–4693.
- Georgakilas, V.; Otyepka, M.; Bourlino, A. B.; Chandra, V.; Kim, N.; Kemp, K. C.; Hobza, P.; Zboril, R.; Kim, K. S. *Chem Rev* **2012**, *112*, 6156–6214.
- Englert, J. M.; Röhl, J.; Schmidt, C. D.; Graupner, R.; Hundhausen, M.; Hauke, F.; Hirsch, A. *Advanced Materials* **2009**, *21*, 4265–4269.
- Backes, C.; Schmidt, C. D.; Rosenlechner, K.; Hauke, F.; Coleman, J. N.; Hirsch, A. *Advanced Materials* **2010**, *22*, 788–802.
- Yang, H.; Hernandez, Y.; Schlierf, A.; et al. *Carbon* **2013**, *53*, 357–365.
- Parviz, D.; Das, S.; Ahmed, H. S. T.; Irin, F.; Bhattacharia, S.; Green, M. J. *ACS Nano* **2012**, *6*, 8857–8867.
- Su, Q.; Pang, S.; Alijani, V.; Li, C.; Feng, X.; Muellen, K. *Advanced Materials* **2009**, *21*, 3191.
- An, X.; Butler, T. W.; Washington, M.; Nayak, S. K.; Kar, S. *ACS Nano* **2011**, *5*, 1003–1011.
- Geng, J.; Kong, B.-S.; Yang, S. B.; Jung, H.-T. *Chemical Communications* **2010**, *46*, 5091–5093.
- Xu, Y.; Zhao, L.; Bai, H.; Hong, W.; Li, C.; Shi, G. *Journal of the American Chemical Society* **2009**, *131*, 13490–13497.
- Xu, Y. F.; Liu, Z. B.; Zhang, X. L.; Wang, Y.; Tian, J. G.; Huang, Y.; Ma, Y. F.; Zhang, X. Y.; Chen, Y. S. *Adv. Mater.* **2009**, *21*, 1275.
- Tu, W.; Lei, J.; Zhang, S.; Ju, H. *Chemistry-a European Journal* **2010**, *16*, 10771–10777.
- Geng, J.; Jung, H.-T. *Journal of Physical Chemistry C* **2010**, *114*, 8227–8234.
- Zhang, X. Y.; Huang, Y.; Wang, Y.; Ma, Y. F.; Liu, Z. F.; Chen, Y. S. *Carbon* **2009**, *47*, 334–337.
- Melucci, M.; Treossi, E.; Ortolani, L.; Giambastiani, G.; Morandi, V.; Klar, P.; Casiraghi, C.; Samori, P.; Palermo, V. *Journal of Materials Chemistry* **2010**, *20*, 9052–9060.
- Melucci, M.; Durso, M.; Zambianchi, M.; et al. *Journal of Materials Chemistry* **2012**, *22*, 18237–18243.
- Liu, Y. S.; Zhou, J. Y.; Zhang, X. L.; Liu, Z. B.; Wan, X. J.; Tian, J. G.; Wang, T.; Chen, Y. S. *Carbon* **2009**, *47*, 3113–3121.
- Saxena, A. P.; Deepa, M.; Joshi, A. G.; Bhandari, S.; Srivastava, A. K. *ACS Applied Materials & Interfaces* **2011**, *3*, 1115–1126.
- Quintana, M.; Montellano, A.; Castillo, A. E. D.; Van Tendeloo, G.; Bittencourt, C.; Prato, M. *Chemical Communications* **2011**, *47*, 9330–9332.
- Su, C.; Tandiana, R.; Balapanuru, J.; Tang, W.; Pareek, G.; Nai, C. T.; Hayashi, T.; Loh, K. P. *Journal of the American Chemical Society* **2015**, *137*, 685.
- He, S. J.; Song, B.; Li, D.; et al. *Advanced Functional Materials* **2009**, *20*, 453–459.
- Patil, A. J.; Vickery, J. L.; Scott, T. B.; Mann, S. *Advanced Materials* **2009**, *21*, 3159.
- Yang, H.; Withers, F.; Gebremedhn, E.; et al. *2D Materials* **2014**, *1*, 011012.
- Schlierf, A.; Cha, K.; Schwab, M. G.; Samori, P.; Palermo, V. *2D Materials* **2014**, *1*, 035006.
- Sinitskii, A.; Dimiev, A.; Corley, D. A.; Fursina, A. A.; Kosynkin, D. V.; Tour, J. M. *ACS Nano* **2010**, *4*, 1949–1954.
- Niyogi, S.; Bekyarova, E.; Itkis, M. E.; et al. *Nano Letters* **2010**, *10*, 4061–4066.
- Coletti, C.; Riedl, C.; Lee, D. S.; Krauss, B.; Patthey, L.; von Klitzing, K.; Smet, J. H.; Starke, U. *Phys. Rev. B* **2010**, *81*, #235401.
- Zhang, Y. H.; Zhou, K. G.; Xie, K. F.; Zeng, J.; Zhang, H. L.; Peng, Y. *Nanotechnology* **2010**, *21*, #065201.
- Dong, X. C.; Fu, D. L.; Fang, W. J.; Shi, Y. M.; Chen, P.; Li, L. J. *Small* **2009**, *5*, 1422–1426.
- Melucci, M.; Treossi, E.; Ortolani, L.; Giambastiani, G.; Morandi, V.; Klar, P.; Casiraghi, C.; Samori, P.; Palermo, V. *Journal of Materials Chemistry* **2010**, *20*, 9052–9060.
- Treossi, E.; Melucci, M.; Liscio, A.; Gazzano, M.; Samori, P.; Palermo, V. *Journal of the American Chemical Society* **2009**, *131*, 15576–15577.
- Kim, J.; Cote, L. J.; Kim, F.; Huang, J. X. *Journal of the American Chemical Society* **2010**, *132*, 260–267.
- Gaudreau, L.; Tielrooij, K. J.; Prawiroatmodjo, G. E. D. K.; Osmond, J.; de Abajo, F. J. G.; Koppens, F. H. L. *Nano Letters* **2013**, *13*, 2030–2035.
- Ciesielski, A.; Haar, S.; El Gemayel, M.; et al. *Angewandte Chemie-International Edition* **2014**, *53*, 10355–10361.
- El Gemayel, M.; Haar, S.; Liscio, F.; et al. *Advanced Materials* **2014**, *26*, 4814.
- Mativetsky, J. M.; Liscio, A.; Treossi, E.; Orgiu, E.; Zanelli, A.; Samori, P.; Palermo, V. *Journal of the American Chemical Society* **2011**, *133*, 14320–14326.
- Mativetsky, J. M.; Treossi, E.; Orgiu, E.; Melucci, M.; Veronese, G. P.; Samori, P.; Palermo, V. *Journal of the American Chemical Society* **2010**, *132*, 14130–14136.
- Liu, Y.; Yuan, L.; Yang, M.; et al. *Nature Communications* **2014**, *5*, #5461.
- Tsouf, T.; Tuci, G.; Caporali, S.; Gournis, D.; Giambastiani, G. *Carbon* **2013**, *59*, 100–108.
- Ji, L. W.; Tan, Z. K.; Kuykendall, T.; An, E. J.; Fu, Y. B.; Battaglia, V.; Zhang, Y. G. *Energy & Environmental Science* **2011**, *4*, 3611–3616.
- Chen, Z. P.; Ren, W. C.; Gao, L. B.; Liu, B. L.; Pei, S. F.; Cheng, H. M. *Nature Materials* **2011**, *10*, 424–428.
- Xia, Z. Y.; Wei, D.; Anitowska, E.; et al. *Carbon* **2015**, *84*, 254–262.
- Yao, H.-B.; Ge, J.; Wang, C.-F.; Wang, X.; Hu, W.; Zheng, Z.-J.; Ni, Y.; Yu, S.-H. *Advanced Materials* **2013**, *25*, 6692–6698.
- Mecklenburg, M.; Schuchardt, A.; Mishra, Y. K.; Kaps, S.; Adlung, R.; Lotnyk, A.; Kienle, L.; Schulte, K. *Advanced Materials* **2012**, *24*, 3486–3490.
- Zou, J.; Kim, F. *Nature Communications* **2014**, *5*, #5254.
- Barg, S.; Perez, F. M.; Ni, N.; et al. *Nature Communications* **2014**, *5*, #4328.
- Wei, W.; Yang, S.; Zhou, H.; Lieberwirth, I.; Feng, X.; Muellen, K. *Advanced Materials* **2013**, *25*, 2909–2914.
- Wu, Z. S.; Yang, S. B.; Sun, Y.; Parvez, K.; Feng, X. L.; Mullen, K. *Journal of the American Chemical Society* **2012**, *134*, 9082–9085.
- Jin, Z.-Y.; Lu, A.-H.; Xu, Y.-Y.; Zhang, J.-T.; Li, W.-C. *Advanced Materials* **2014**, *26*, 3700–3705.
- Luo, B.; Wang, B.; Liang, M.; Ning, J.; Li, X.; Zhi, L. *Advanced Materials* **2012**, *24*, 1405–1409.
- Han, S.; Wu, D.; Li, S.; Zhang, F.; Feng, X. *Advanced Materials* **2014**, *26*, 849–864.

## Graphite

For a complete list of available materials, visit [aldrich.com/graphite](http://aldrich.com/graphite).

Name	Form	Particle Size (mm)	Purity (%)	Prod. No.
Graphite	flakes	+100 mesh ( $\geq 75\%$ min)	-	332461-2.5KG 332461-12KG
	rod	L 150 diam. 3	99.999 trace metals basis	496537-43.5G
	rod	L 150 diam. 6	99.995 trace metals basis	496553-180.7G
	powder	<150 $\mu\text{m}$	99.99 trace metals basis	496588-113.4G
	powder	<45 $\mu\text{m}$	$\geq 99.99$ trace metals basis	496596-113.4G
	powder	<20 $\mu\text{m}$	-	282863-25G 282863-1KG
	powder	100 nm (average width, TEM) 2.5 $\mu\text{m}$ (average length, TEM) D $\times$ L 50-250 nm $\times$ 0.5-5 $\mu\text{m}$	98 carbon basis	698830-1G

## Graphene Oxide and Reduced Graphene Oxide

For a complete list of available materials, visit [aldrich.com/graphene](http://aldrich.com/graphene).

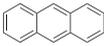
Name	Form	Description	Prod. No.
Graphene oxide	flakes	sheets	763713-250MG 763713-1G
	powder	15-20 sheets 4-10% edge-oxidized	796034-1G
	dispersion in H <sub>2</sub> O	2 mg/mL	763705-25ML 763705-100ML
	dispersion in H <sub>2</sub> O	4 mg/mL, Dispersibility: Polar solvents Monolayer content (measured in 0.5mg/mL): >95%	777676-50ML 777676-200ML
	dispersion in H <sub>2</sub> O	1 mg/mL, 15-20 sheets, 4-10% edge-oxidized	794341-50ML 794341-200ML
	film	4cm (diameter) x 12-15mm (thickness), non-conductive	798991-1EA
	Graphene oxide nanocolloids	dispersion in H <sub>2</sub> O	2 mg/mL
Graphene oxide, ammonia functionalized	dispersion in H <sub>2</sub> O	1 mg/mL	791520-25ML 791520-100ML
Reduced graphene oxide	powder	chemically reduced	777684-250MG 777684-500MG

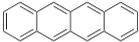
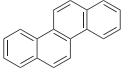
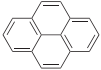
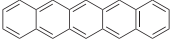
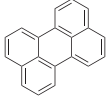
## Precursors of 2D Materials

For a complete list of available materials, visit [aldrich.com/ceramics](http://aldrich.com/ceramics).

Name	Form	Avg. Part. Size	Purity (%)	Prod. No.
Molybdenum(IV) selenide	powder	-325 mesh	99.9 trace metals basis	778087-5G
Molybdenum(IV) sulfide	powder	<2 $\mu\text{m}$	99	234842-100G 234842-500G
	powder	$\sim 6$ $\mu\text{m}$ (max. 40 $\mu\text{m}$ )	-	69860-100G 69860-500G
Tungsten(IV) sulfide	nanopowder	90 nm (SEM)	99 trace metals basis	790583-5G
	powder	2 $\mu\text{m}$	99	243639-50G
Boron nitride	nanopowder	<150 nm (BET)	99 trace metals basis	790532-10G
	powder	$\sim 1$ $\mu\text{m}$	98	255475-50G 255475-250G
Manganese(IV) oxide	powder and chunks	-	$\geq 99.99$ trace metals basis	529664-5G 529664-25G

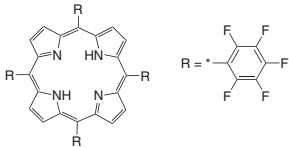
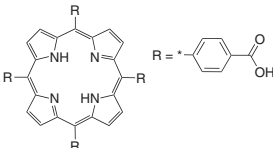
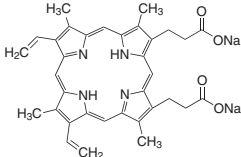
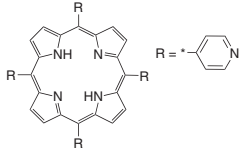
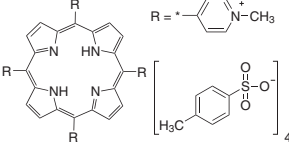
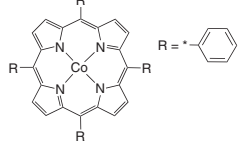
## Polycyclic Aromatic Hydrocarbons (PAHs)

Structure	Name	Purity (%)	Prod. No.
	Anthracene	$\geq 99$ sublimed grade	694959-5G 694959-25G
	Phenanthrene	$\geq 99.5$ sublimed grade	695114-1G 695114-5G

Structure	Name	Purity (%)	Prod. No.
	Benz[ <i>b</i> ]anthracene	99.99 sublimed grade	698415-1G
	Chrysene	98	245186-500MG 245186-1G
	Triphenylene	98	T82600-1G
	Pyrene	99 sublimed grade 98	571245-1G 185515-1G 185515-25G 185515-100G
	Pentacene	≥99.995 triple-sublimed grade ≥99.9 sublimed grade	698423-500MG 684848-1G
	Perylene	≥99.5 sublimed grade	394475-1G 394475-5G

## Porphyrins

For a complete list of available materials, visit [aldrich.com/porphyrins](http://aldrich.com/porphyrins).

Structure	Name	Purity (%)	Absorption	Prod. No.
	5,10,15,20-Tetrakis(pentafluorophenyl)porphyrin	≥90.0	$\lambda_{\max} = 416 \text{ nm}$ $\lambda_{\max} = 507 \text{ nm}$	252921-100MG 252921-1G
	4,4'4''-(Porphine-5,10,15,20-tetrayl)tetrakis(benzoic acid)	-	$\lambda_{\max} = 411 \text{ nm}$	379077-250MG 379077-1G
	Protoporphyrin IX disodium salt	≥90	$\lambda_{\max} = 406 \text{ nm}$	258385-250MG 258385-1G 258385-5G
	5,10,15,20-Tetra(4-pyridyl)-21H,23H-porphine	97	$\lambda_{\max} = 412 \text{ nm}$	257613-1G 257613-5G
	5,10,15,20-Tetrakis(1-methyl-4-pyridinio)porphyrin tetra( <i>p</i> -toluenesulfonate)	-	$\lambda_{\max} = 421 \text{ nm}$	323497-100MG 323497-250MG
	5,10,15,20-Tetraphenyl-21H,23H-porphine cobalt(II)	-	$\lambda_{\max} = 409 \text{ nm}$ $\lambda_{\max} = 524 \text{ nm}$	252190-500MG

## Porphyrins (cont'd)

Structure	Name	Purity (%)	Absorption	Prod. No.
	5,10,15,20-Tetrakis(4-methoxyphenyl)-21H,23H-porphine cobalt(II)	≥96.0	$\lambda_{\text{max}} = 417 \text{ nm}$ $\lambda_{\text{max}} = 530 \text{ nm}$	275867-1G 275867-10G
	5,10,15,20-Tetraphenyl-21H,23H-porphine iron(III) chloride	≥94	$\lambda_{\text{max}} = 418 \text{ nm}$	259071-500MG
	5,10,15,20-Tetrakis(pentafluorophenyl)-21H,23H-porphyrin iron(III) chloride	≥95	$\lambda_{\text{max}} = 498 \text{ nm}$ $\lambda_{\text{max}} = 415 \text{ nm}$	252913-100MG
	5,10,15,20-Tetraphenyl-21H,23H-porphine manganese(III) chloride	95	$\lambda_{\text{max}} = 475 \text{ nm}$ $\lambda_{\text{max}} = 583 \text{ nm}$	254754-500MG
	5,10,15,20-Tetraphenyl-21H,23H-porphine ruthenium(II) carbonyl	-	$\lambda_{\text{max}} = 410 \text{ nm}$	392448-100MG 392448-1G

## Polythiophenes

For a complete list of available materials, visit [aldrich.com/polythiophene](http://aldrich.com/polythiophene).

Structure	Name	Regioregularity	Mol. Wt.	Prod. No.
	Poly(3-butylthiophene-2,5-diyl)	regioregular	$M_w$ 54,000 (typical)	495336-1G
		regiorandom	-	511420-1G
	Poly(3-hexylthiophene-2,5-diyl)	regioregular	average $M_n$ 54,000-75,000	698997-250MG 698997-1G 698997-5G
		regioregular	average $M_n$ 15,000-45,000	698989-250MG 698989-1G 698989-5G
		regioregular	-	445703-1G
		regiorandom	-	510823-1G
	Poly(3-octylthiophene-2,5-diyl)	regioregular	$M_n$ ~34,000	445711-1G
		regioregular	average $M_n$ ~25,000	682799-250MG
	Poly(3-decylthiophene-2,5-diyl)	regioregular	average $M_n$ ~30,000 average $M_w$ ~42,000	495344-1G
	Poly(3-dodecylthiophene-2,5-diyl)	regioregular	average $M_w$ ~60,000	450650-1G
		regioregular	average $M_w$ ~27,000	682780-250MG

# GRAPHENE-BASED COMPOSITES

## AND THEIR UNIQUE RENEWABLE ENERGY APPLICATIONS



Wen Qian, Andrew Y. Wang\*  
Ocean NanoTech, LLC, San Diego, CA 92126, USA  
\*Email: awang@oceannanotech.com

### Introduction

Graphene is a unique two-dimensional (2D) structure of monolayer carbon atoms packed into a dense honeycomb crystal that has attracted great interest due to its diverse and fascinating properties.<sup>1</sup> Since it was first isolated in monolayer form in 2004,<sup>2</sup> more and more mechanical, physical, and chemical routes have been developed to produce graphene. Of these diverse methods, chemical production of graphene is currently the lowest-cost method and is becoming a preferred mass production method. Currently, three major carbon sources are used as starting materials for the chemical production of graphene: 1) chemical reduction of graphite oxide (GO);<sup>3,4</sup> 2) sieved graphite powder (SGP);<sup>5-8</sup> and 3) expanded graphite (EG).<sup>9-12</sup> Although chemically reduced GO (rGO) (Aldrich Prod. No. 777684) contains a significant number of oxygen-rich functional groups favorable for surface decoration, the large number of defects that exist in the graphene lattice is irreversible.<sup>13-16</sup> Comparatively, graphene sheets exfoliated from EG and SGP exhibit high electrical conductivity due to relatively low crystallographic defect densities.<sup>17</sup>

In view of its high surface area-to-mass ratio (2,600 m<sup>2</sup>/g),<sup>18</sup> superior charge-carrier mobility (2×10<sup>5</sup> cm<sup>2</sup>/V s),<sup>19</sup> excellent tensile strength of 130 GPa,<sup>20</sup> and thermal conductivity of (4.84~5.30)×10<sup>3</sup> W/m-K,<sup>21</sup> graphene is considered an ideal substrate for growing and anchoring various metal and metal oxide nanocrystals (NCs) to form high-performance nanocomposites. The manufacturing of such graphene hybrids requires that graphene sheets not only be produced inexpensively and in large quantities, but also that the attached metal/metal oxide NCs be incorporated and homogeneously distributed on the graphene surface. This article highlights the production, structure, and performance of three different types of graphene-based composites, including: 1) graphene decorated with transition metal (Fe, Mn, Co) oxide NCs; 2) graphene decorated with noble metal (Pt) and Pt-based alloy; and 3) graphene decorated with TiO<sub>2</sub> NCs. Their specific renewable energy applications—energy storage, energy conversion, and energy production—will also be examined.

### Hybridization of Graphene with Transition Metal (Fe, Mn, Co) Oxides for Energy Storage Devices

Supercapacitors are very promising electrochemical devices for storing and releasing energy. Supercapacitors offer high power density, rapid charge and discharge, superior cycle lifetime, high reliability, and extremely low internal discharge. Over the past few decades, transition metal oxide NCs, such as MnO<sub>x</sub>,<sup>22-24</sup> RuO<sub>2</sub>,<sup>25,26</sup> and Fe<sub>3</sub>O<sub>4</sub>,<sup>27,28</sup> have been thoroughly investigated as electrode materials for use in redox-based pseudocapacitors because of their high theoretical capacitance, abundance, and environmentally friendly nature. However, their high electrical resistance and poor electrochemical reversibility have limited their energy storage capacity for practical applications. Recently, carbon materials such as activated carbon, carbon nanotubes, and graphene have been demonstrated as promising materials for electrochemical double-layer capacitors (EDLC).<sup>29-32</sup> Due to its high specific surface area and high electrical conductivity, graphene can act not only as a substrate for better distribution of transition metal oxide NCs, but also as a direct conductive path for rapid electron transmission. The hybrid of conductive graphene with transition metal oxide NCs has generated interest because of the potential for a synergistic effect on device performance. The well-dispersed transition metal oxide NCs on the graphene can effectively prevent the stacking of graphene sheets, leading to higher available surface areas for the charge storage. The use of high-quality exfoliated graphene as a conductive substrate not only provides efficient electron transfer channels for attached NCs, but also contributes double-layer capacitance to the overall energy storage and, therefore, has great potential for improving the energy storage capacity of supercapacitors. During the past decades, various methods have been developed to hybridize transition metal oxide NCs on GO.<sup>33-40</sup> Yan et al. developed a solvothermal approach for decorating the reduced GO with Fe<sub>3</sub>O<sub>4</sub> NCs and proved that the capacitance of composites is much higher than that of pure reduced GO and Fe<sub>3</sub>O<sub>4</sub> NCs.<sup>36</sup> Wang et al. fabricated GO/MnO<sub>2</sub> nanocomposites via a simple chemical route in a water-isopropyl alcohol system and then demonstrated the composite can act as electrode material for supercapacitors.<sup>38</sup> Qin et al. fabricated reduced GO/MnO<sub>2</sub> composite electrodes by *in situ* anodic electrodeposition.<sup>40</sup>

The aforementioned hybrids have shown to act as promising electrode materials for supercapacitor applications. However, all of these methods used GO or reduced GO as the precursor, and they are known to possess high densities of irreversible structural defects in their lattices. Another drawback of these potential supercapacitor materials is that the particle size and loading density of attached NPs cannot be precisely controlled. Moreover, these synthetic techniques require multiple complicated

synthetic steps and additionally require the use of surfactants. Qian et al. developed a one-step synthetic procedure to both produce the transition metal oxide NCs and attach the NCs to the graphene surface.<sup>41</sup> High-quality graphene hybrid with attached magnetite ( $\text{Fe}_3\text{O}_4$ ) NCs were readily prepared using a simple solvothermal process. Iron (III) acetylacetonate (Aldrich Prod. No. 517003) and expanded graphite were employed as precursors, and ethanol was used as a safe and harmless reaction medium. No surfactant was involved in the preparation of these nanophase composite materials. Experimental results demonstrated that this simple and environmentally friendly chemical process could be extended to hybridize other metal oxide NCs, such as  $\text{Mn}_3\text{O}_4$  and  $\text{CoO}$ . TEM analyses indicated that the particle size and coating density of  $\text{Fe}_3\text{O}_4$  and  $\text{Mn}_3\text{O}_4$  could be readily tailored by varying reaction time, as shown in Figure 1.

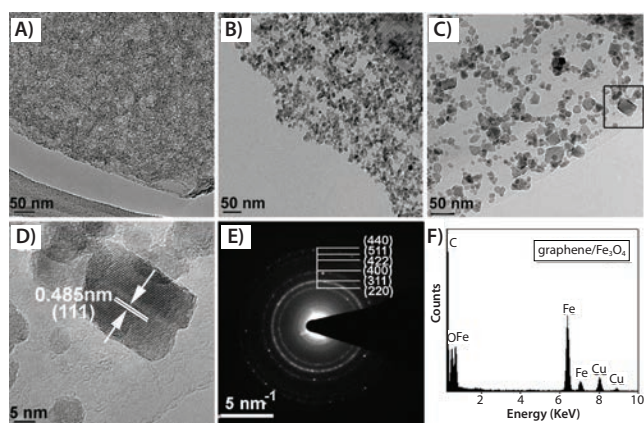


**Figure 1.** TEM analysis of graphene/ $\text{Fe}_3\text{O}_4$  composites prepared by solvothermal reaction at  $180^\circ\text{C}$  at varying reaction times of 4 h (A), 8 h (B), and 16 h (C); D) HRTEM image of boxed area of (C); E) the corresponding SAED pattern; F) typical EDS pattern of the attached  $\text{Fe}_3\text{O}_4$  NCs.

The electrochemical performance of graphene/ $\text{Mn}_3\text{O}_4$  (Aldrich Prod. No. 803723), graphene/ $\text{Fe}_3\text{O}_4$  (Aldrich Prod. No. 803715) and graphene/ $\text{CoO}$  composites as supercapacitor anode materials was also investigated. These hybrids were found to exhibit enhanced capacitance compared to

that of pristine graphene and pure NCs, and have high current density while maintaining long-term cycling stability (Figure 2).

## Hybridization of Graphene with Noble Metals and Alloys for Energy Conversion Devices

Direct methanol fuel cells (DMFCs) are becoming attractive competitors to traditional fuels for transportation and electrical power generation—especially for mobile and portable applications—due to their exciting performance advantages.<sup>42–44</sup> Currently, XC-72 carbon black is the most widely used carbon support for fuel cell catalysts because of its good balance between electronic conductivity and high surface area. However, commercial carbon-supported platinum (Pt/C) fuel cells have serious deficiencies, including the slow rate of oxygen reduction reaction (ORR), the high cost of platinum, the cross-over of methanol from the anode to the cathode through the proton exchange membranes, the vulnerability of the reaction to be poisoned by carbon monoxide (CO), and the rapid loss of catalytic activity caused by the existence of halide ions, as well as catalyst particle aggregation and deformation.<sup>45,46</sup> As a result, the lifetime of such a fuel cell is rather poor. The introduction of a second, less expensive transition metal such as Fe, Ni, Co, Cr, Pd, Ru, or Bi to form Pt-based alloys has proven to enhance electrocatalytic activity for ORRs, taking advantage of the increased Pt d-band vacancy and more favorable Pt-Pt interatomic distance in comparison with using Pt alone.<sup>47–49</sup> In order to maximize the catalytic activity of Pt and to minimize expensive Pt material consumption, it is necessary to prepare Pt NCs with ultrafine sizes. Obviously, the highly accessible surface area and the number of edge and corner atoms of the small NCs would greatly improve the catalytic activity. To avoid detrimental aggregation of the small NCs, the existing methods of synthesizing small NCs rely on surfactants<sup>50</sup> and ligands<sup>51</sup> to stabilize the NCs. The drawback of the presence of surfactants in the resulting product is the seriously decreased electrocatalytic performance. Therefore, selecting an ideal substrate, then hybridizing it with uniformly dispersed Pt NCs and Pt-M alloys—but without the use of a surfactant or stabilizer—is urgently needed for the advancement of DMFCs.

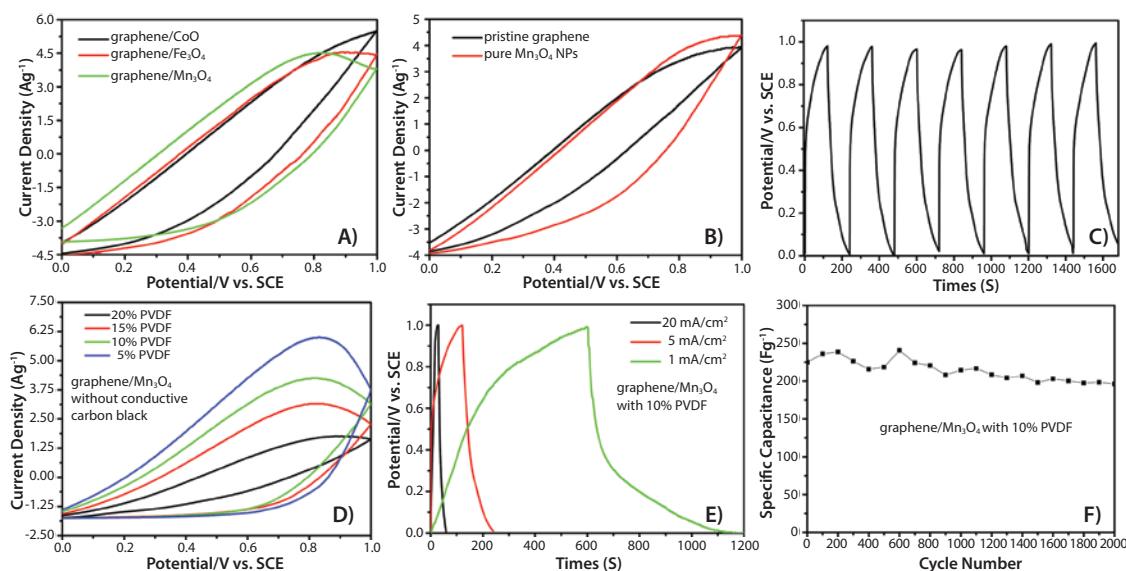


**Figure 2.** A) Cyclic voltammetry (CV) curves of graphene/ $\text{Fe}_3\text{O}_4$  (Aldrich Prod. No. 803715), graphene/ $\text{Mn}_3\text{O}_4$  (Aldrich Prod. No. 803723) and graphene/ $\text{CoO}$  composites, at a scan rate of 10 mV/s in 0.5 M  $\text{NaCl}_{(\text{aq})}$ . B) CV curves of pristine graphene and pure  $\text{Mn}_3\text{O}_4$  NPs at a scan rate of 10 mV/s in 0.5 M  $\text{NaCl}_{(\text{aq})}$ . C) Galvanostatic charge-discharge curve of a graphene/ $\text{Mn}_3\text{O}_4$  composite at a current density of 2 A/g in 0.5 M  $\text{NaCl}_{(\text{aq})}$ . D) CV curves of graphene/ $\text{Mn}_3\text{O}_4$  composites without any conductive carbon black but with different ratio of PVDF as binder, at a scan rate of 10 mV/s in 0.5 M  $\text{NaCl}_{(\text{aq})}$ . E) Galvanostatic charge-discharge curve of a graphene/ $\text{Mn}_3\text{O}_4$  composite at a current density of 1 mA/cm<sup>2</sup>, 5 mA/cm<sup>2</sup> and 20 mA/cm<sup>2</sup> in 0.5 M  $\text{NaCl}_{(\text{aq})}$ . F) Long-term cycling performance of a graphene/ $\text{Mn}_3\text{O}_4$  composite with 10 wt% PVDF.

The emergence of graphene material has enabled a new opportunity to utilize the 2D graphitized planar structure as a substrate for growing and anchoring noble metal NCs and alloy NCs, including Pt,<sup>52–55</sup> Pd,<sup>56,57</sup> PtPd,<sup>58</sup> and PtRu<sup>59</sup> NCs for high-performance electrocatalytic devices. Jalan et al. suggested that the enhanced electrocatalytic activity was due to the contraction of the Pt-Pt interatomic distance by adding a smaller transition metal atom.<sup>60</sup> Ross et al. commented that the roughening of the Pt surface due to the addition of the transition metal could account for the ORR improvement.<sup>61,62</sup> Mukerjee et al. explained this by an increase in Pt d-band vacancies and a more favorable Pt-Pt mean interatomic distance.<sup>63,64</sup> Most of these methods selected H<sub>2</sub>PtCl<sub>6</sub> (Aldrich Prod. Nos. 254029, 520896, etc.) and GO (Aldrich Prod. Nos. 763705, 777676, etc.) as the precursors, which results in rapid loss of catalytic activity. Qian et al. developed a simple, low-cost and environmentally benign process to hybridize exfoliated few-layer graphene sheets with nanocrystalline Pt (Pt/graphene, Aldrich Prod. No. 803693) and Pt-based alloys (PtPd/graphene (Aldrich Prod. No. 803758) and PtCo/graphene (Aldrich Prod. No. 803766)).<sup>65</sup> TEM images indicated that both the resultant single-Pt NCs (Figure 3) as well as alloy (Figure 4) were uniformly distributed on the graphene surface and the loading density easily controlled by the reaction times. Most important, no surfactant and no halide ions were involved in the whole reaction.

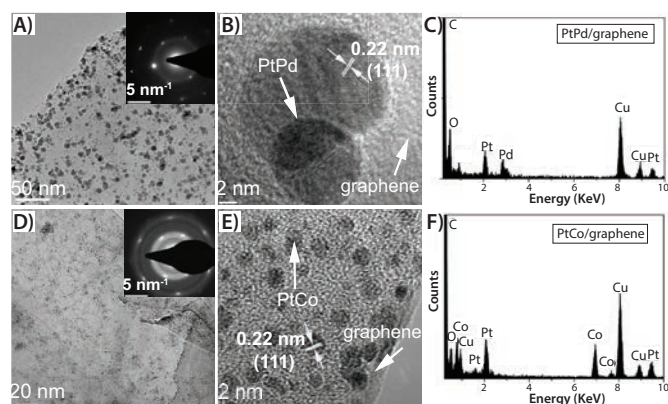


**Figure 4.** TEM analysis of both PtPd/graphene (Aldrich Prod. No. 803758) (A–C) and PtCo/graphene (Aldrich Prod. No. 803766) (D–F) hybrids prepared by a solvothermal reaction at 115 °C for 6 h. A) TEM image of graphene sheet with attached PtPd alloy NCs and corresponding SAED pattern (inset). B) HRTEM micrograph of PtPd/graphene hybrid. C) EDX spectrum of the deposited PtPd alloy NCs. D) TEM image of graphene sheet loaded with PtCo alloy NCs and corresponding SAED pattern (inset). E) HRTEM micrograph of PtCo/graphene hybrid. F) EDX spectrum of the deposited PtCo alloy NCs.

In comparison to commercial Pt/C catalysts, high-quality graphene-supported Pt, PtPd, and PtCo NC hybrids as electrocatalysts demonstrated excellent electron transport, improved efficiency toward methanol oxidation, and improved tolerance to CO poisoning, as well as long-term stability (Figure 5).

## Hybridization of Graphene with TiO<sub>2</sub> for Energy Production Devices

Since hydrogen is commonly regarded as the ultimate clean fuel, the production of hydrogen with solar power plays an important role in clean and renewable energy systems.<sup>66,67</sup> Among all solar-to-hydrogen conversion methods, direct water splitting by a photocatalyst is the most convenient process.<sup>68</sup> Anatase TiO<sub>2</sub> (Aldrich Prod. Nos. 637254, 232033 and 248576), a wide-band-gap semiconducting material, is widely known for use in photocatalysts due to its unique optical and electronic properties. Under UV illumination, electrons are excited from the valence band to the conduction band, forming electron-hole pairs. The purpose of the graphene substrate is to achieve the photocatalytic activity by separating the electron-hole pair, but leaving the hole on the TiO<sub>2</sub> to form the radical, as shown in Figure 6. The photo-generated electron-hole pairs of the TiO<sub>2</sub> have a flash recombination time on the order of 10<sup>-9</sup> s, while

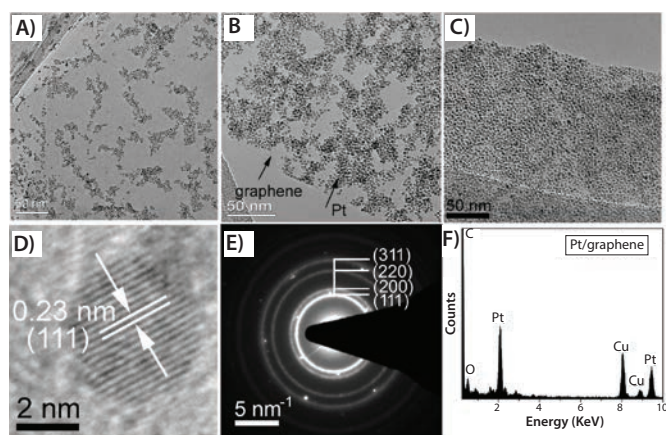


**Figure 3.** TEM analysis of Pt/graphene hybrid (Aldrich Prod. No. 803693) prepared by a solvothermal reaction at 115 °C at varying reaction times of 6 h (A), 12 h (B), and 18 h (C); D) HRTEM micrograph of Pt/graphene hybrid; E) the corresponding SAED pattern; and F) EDX spectrum of deposited Pt NCs.

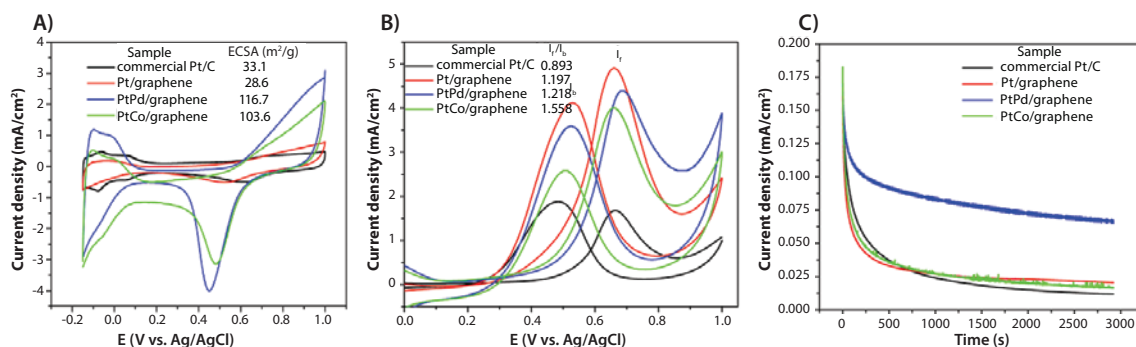


**Figure 5.** A) Cyclic voltammograms of commercial Pt/C (black), Pt/graphene (red), PtPd/graphene (Aldrich Prod. No. 803758) (blue) and PtCo/graphene (Aldrich Prod. No. 803766) (green) in N<sub>2</sub>-saturated 0.5 M HClO<sub>4</sub> electrolyte, at a scanning rate of 50 mV/s. B) Cyclic voltammograms of commercial Pt/C (black), Pt/graphene (red), PtPd/graphene (blue) and PtCo/graphene (green) in 0.5 M CH<sub>3</sub>OH/0.5 M HClO<sub>4</sub> electrolyte, at a scanning rate of 50 mV/s. C) Chronoamperometric curves recorded at 0.65 V (vs Ag/AgCl) of the electrocatalysts in 0.5 M CH<sub>3</sub>OH/0.5 M HClO<sub>4</sub> electrolyte for 3,000 seconds.

the time of chemical interaction of  $\text{TiO}_2$  with adsorbed pollutants is in the range of  $10^{-8}$ – $10^{-3}$  s.<sup>69,70</sup> In addition, the photocatalytic activity of  $\text{TiO}_2$  is strongly dependent on morphology<sup>71,72</sup> and particle size.<sup>73</sup> Experiments have generally shown that reducing pure  $\text{TiO}_2$  particle size would increase photocatalytic activity by decreasing the electron-hole recombination rate in the bulk of the crystal. Once the particle size falls below  $\sim 15$  nm, recombination rates at the surface become the dominant interaction; decreasing the particle size beyond this point leads to a decreased photocatalytic activity.<sup>74</sup> Utilizing the charge separation aspect of  $\text{TiO}_2$ /graphene composites, it is hypothesized that this surface recombination effect can be mitigated, allowing further photocatalytic enhancement through particle size reduction beyond this 15 nm size limit. Graphene/ $\text{TiO}_2$  hybrids have attracted particular interest for this reason and have been shown to provide drastic increases in photocatalytic and photovoltaic performance when compared to lone  $\text{TiO}_2$  catalysts.<sup>75,76</sup>

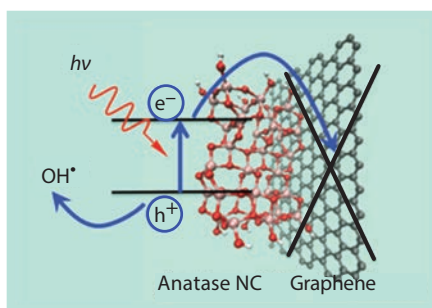


**Figure 6.** Schematic of the separation of a photoexcited electron-hole pair in a  $\text{TiO}_2$  NC.

$\text{TiO}_2$  NCs have long been studied due to their potential photocatalytic applications in water purification and hydrogen-energy production.<sup>77–79</sup> Both theoretical prediction and experimental results indicate that (001) facets of anatase  $\text{TiO}_2$  are much more reactive than other thermodynamically stable facets.<sup>80–83</sup> Since the pioneering work by Lu et al. on the synthesis of micrometer-sized anatase crystals with a large percentage of (001) facets,<sup>80</sup> there has been remarkable interest in the controlled synthesis of anatase crystals with varied percentages of exposed (001) facets, such as truncated tetragonal bipyramids and square sheets.<sup>82–85</sup> Hybridizing shape-controlled  $\text{TiO}_2$  NCs on the surface of graphene sheets may not only favor the dispersion of NCs, but also contribute to the improvement of photocatalysis due to the unique electron mobility. Zhang et al. was the first to prepare a chemically bonded  $\text{TiO}_2$  (P25)-graphene composite photocatalyst by hydrothermal reaction.<sup>86</sup> Since then, many efforts using the synthesis of GO/ $\text{TiO}_2$  composites have been made in order to increase the efficiency of photocatalysis,<sup>87–89</sup> however, none of these efforts used exfoliated crystalline graphene as a precursor. Recently, Qian et al.<sup>90</sup> successfully hybridized highly conductive graphene with nanocubic  $\text{TiO}_2$  NCs. These composite materials clearly show a lattice spacing of 0.35 nm corresponding to the (101) plane of anatase  $\text{TiO}_2$ , as can be seen in **Figures 7A–B**. Considering that anatase  $\text{TiO}_2$  adopts a tetragonal structure with lattice parameters  $a = b = 0.377$  nm and  $c = 0.950$  nm, the square surface in the crystal structure can be assigned to (001) facets.

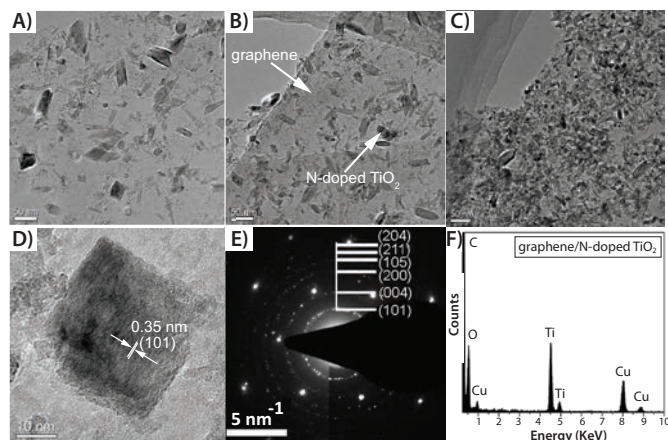


**Figure 7.** TEM analysis of N-doped  $\text{TiO}_2$ /graphene prepared at low temperature of 180 °C at varying reaction times of **A)** 7 h, **B)** 14 h, and **C)** 21 h; **D)** HRTEM image of deposited N-doped  $\text{TiO}_2$  NCs; **E)** corresponding SAED pattern; **F)** typical EDX pattern of deposited N-doped  $\text{TiO}_2$  NCs.

## Conclusion

The fabrication of novel graphene-based composites by combining high-quality graphene with various metal and metal oxide NCs has proven to be a very promising approach for developing improved clean energy devices. These new graphene-based metal and metal oxides are expected to have an impact in three categories within the clean energy arena: energy storage (supercapacitors), energy conversion (fuel cells), and energy production (hydrogen generation via water splitting). Once technological and performance issues are fully resolved, these nanocomposites have the potential to be manufactured on an industrial scale and to help address significant global economic and environmental challenges.

## References

- Geim, A. K.; Novoselov, K. S. *Nat. Mater.* **2007**, *6* (3), 183–191.
- Novoselov, K. S.; Geim, A. K.; Morozov, S. V.; Jiang, D.; Zhang, Y.; Dubonos, S. V.; Grigorieva, I. V.; Firsov, A. A. *Science* **2004**, *306*, (5696), 666–669.
- Si, Y.; Samulski, E. T. *Nano Lett.* **2008**, *8*, 1679–1682.
- Xu, Y. X.; Bai, H.; Lu, G. W.; Li, C.; Shi, G. Q. *J. Am. Chem. Soc.* **2008**, *130*, 5856–5857.
- Hernandez, Y.; Nicolosi, V.; Lotya, M.; Blighe, F. M.; Sun, Z. Y.; De, S.; McGovern, I. T.; Holland, B.; Byrne, M.; Gun'ko, Y. K.; Boland, J. J.; Niraj, P.; Duesberg, G.; Krishnamurthy, S.; Goodhue, R.; Hutchison, J.; Scardaci, V.; Ferrari, A. C.; Coleman, J. N. *Nat. Nanotechnol.* **2008**, *3*, 563–568.
- Valles, C.; Drummond, C.; Saadaoui, H.; Furtado, C. A.; He, M.; Roubeau, O.; Ortolani, L.; Monthieux, M.; Penicaud, A. *J. Am. Chem. Soc.* **2008**, *130*, 15802–15804.
- Liu, N.; Luo, F.; Wu, H. X.; Liu, Y. H.; Zhang, C.; Chen, J. *Adv. Funct. Mater.* **2008**, *18*, 1518–1525.
- Viculis, L. M.; Mack, J. J.; Kaner, R. B. *Science* **2003**, *299*, 1361–1361.
- Li, X. L.; Wang, X. R.; Zhang, L.; Lee, S. W.; Dai, H. J. *Science* **2008**, *319*, 1229–1232.
- Li, X. L.; Zhang, G. Y.; Bai, X. D.; Sun, X. M.; Wang, X. R.; Wang, E.; Dai, H. J. *Nat. Nanotechnol.* **2008**, *3*, 538–542.
- Hao, R.; Qian, W.; Zhang, L. H.; Hou, Y. L. *Chem. Commun.* **2008**, 6576–6578.
- Qian, W.; Hao, R.; Hou, Y. L.; Tian, Y.; Shen, C. M.; Gao, H. J.; Liang, X. L. *Nano Res.* **2009**, *2* (9), 706–712.
- Fan, X. B.; Peng, W. C.; Li, Y.; Li, X. Y.; Wang, S. L.; Zhang, G. L.; Zhang, F. B. *Adv. Mater.* **2008**, *20*, 4490–4493.
- Tung, V. C.; Allen, M. J.; Yang, Y.; Kaner, R. B. *Nat. Nanotechnol.* **2009**, *4*, 25–29.
- Park, S.; An, J. H.; Piner, R. D.; Jung, I.; Yang, D. X.; Velamakanni, A.; Nguyen, S. T.; Ruoff, R. S. *Chem. Mat.* **2008**, *20*, 6592–6594.
- Stankovich, S.; Piner, R. D.; Chen, X. Q.; Wu, N. Q.; Nguyen, S. T.; Ruoff, R. S. *J. Mater. Chem.* **2006**, *16*, 155–158.
- Zhu, J. *Nat. Nanotechnol.* **2008**, *3*, 528–529.

- (18) Stankovich, S.; Dikin, D. A.; Dommett, G. H. B.; Kohlhaas, K. M.; Zimney, E. J.; Stach, E. A.; Piner, R. D.; Nguyen, S. T.; Ruoff, R. S. *Nature* **2006**, *442* (7100), 282–286.
- (19) Du, X.; Skachko, I.; Barker, A.; Andrei, E. Y. *Nat. Nanotechnol.* **2008**, *3* (8), 491–495.
- (20) Lee, C.; Wei, X. D.; Kysar, J. W.; Hone, J. *Science* **2008**, *321* (5887), 385–388.
- (21) Balandrin, A. A.; Ghosh, S.; Bao, W. Z.; Calizo, I.; Teweldebrhan, D.; Miao, F.; Lau, C. N. *Nano Lett.* **2008**, *8* (3), 902–907.
- (22) Wei, W. F.; Cui, X. W.; Chen, W. X.; Ivey, D. G. *Chem. Soc. Rev.* **2011**, *40* (3), 1697–1721.
- (23) Hu, C. C.; Wu, Y. T.; Chang, K. H. *Chem. Mater.* **2008**, *20* (9), 2890–2894.
- (24) Toupin, M.; Brousse, T.; Belanger, D. *Chem. Mater.* **2004**, *16* (16), 3184–3190.
- (25) Liu, T. C.; Pell, W. G.; Conway, B. E. *Electrochim. Acta* **1997**, *42* (23–24), 3541–3552.
- (26) Subramanian, V.; Hall, S. C.; Smith, P. H.; Rambabu, B. *Solid State Ion.* **2004**, *175* (1–4), 511–515.
- (27) Cottineau, T.; Toupin, M.; Delahaye, T.; Brousse, T.; Belanger, D. *Applied Physics a-Materials Science & Processing* **2006**, *82* (4), 599–606.
- (28) Wu, N. L.; Wang, S. Y.; Han, C. Y.; Wu, D. S.; Shiue, L. R. *J. Power Sources* **2003**, *113* (1), 173–178.
- (29) Miller, J. R.; Outlaw, R. A.; Holloway, B. C. *Science* **2010**, *329* (5999), 1637–1639.
- (30) Futaba, D. N.; Hata, K.; Yamada, T.; Hiraoka, T.; Hayamizu, Y.; Kakudate, Y.; Tanaie, O.; Hatori, H.; Yumura, M.; Iijima, S. *Nat. Mater.* **2006**, *5* (12), 987–994.
- (31) Frackowiak, E.; Beguin, F. *Carbon* **2001**, *39* (6), 937–950.
- (32) Zhu, Y. W.; Murali, S.; Stoller, M. D.; Ganesh, K. J.; Cai, W. W.; Ferreira, P. J.; Pirkle, A.; Wallace, R. M.; Cyhosh, K. A.; Thommes, M.; Su, D.; Stach, E. A.; Ruoff, R. S. *Science* **2011**, *332* (6037), 1537–1541.
- (33) Wang, H. L.; Robinson, J. T.; Diankov, G.; Dai, H. *J. Am. Chem. Soc.* **2010**, *132* (10), 3270–3271.
- (34) Cong, H. P.; He, J. J.; Lu, Y.; Yu, S. H. *Small* **2010**, *6* (2), 169–173.
- (35) He, H. K.; Gao, C. *ACS Applied Materials & Interfaces* **2010**, *2* (11), 3201–3210.
- (36) Shi, W. H.; Zhu, J. X.; Sim, D. H.; Tay, Y. Y.; Lu, Z. Y.; Zhang, X. J.; Sharma, Y.; Srinivasan, M.; Zhang, H.; Hng, H. H.; Yan, Q. Y. *J. Mater. Chem.* **2011**, *21* (10), 3422–3427.
- (37) Li, B. J.; Cao, H. Q.; Shao, J.; Qu, M. Z.; Warner, J. H. *J. Mater. Chem.* **2011**, *21* (13), 5069–5075.
- (38) Chen, S.; Zhu, J. W.; Wu, X. D.; Han, Q. F.; Wang, X. *ACS Nano* **2010**, *4* (5), 2822–2830.
- (39) Wu, Z. S.; Ren, W. C.; Wang, D. W.; Li, F.; Liu, B. L.; Cheng, H. M. *ACS Nano* **2010**, *4* (10), 5835–5842.
- (40) Cheng, Q.; Tang, J.; Ma, J.; Zhang, H.; Shinya, N.; Qin, L.-C. *Carbon* **2011**, *49* (9), 2917–2925.
- (41) Qian, W.; Chen, Z.; Cottingham, S.; Swartz, N.; Goforth, A.; Clare, T.; Jiao, J. *Green Chem.* **2012**, *14*, 371–377.
- (42) Wasmus, S.; Kuver, A. *J. Electroanal. Chem.* **1999**, *461* (1–2), 14–31.
- (43) Arico, A. S.; Srinivasan, S.; Antonucci, V. *Fuel Cells* **2001**, *1* (2), 133–161.
- (44) Liu, H. S.; Song, C. J.; Zhang, L.; Zhang, J. J.; Wang, H. J.; Wilkinson, D. P. *J. Power Sources* **2006**, *155* (2), 95–110.
- (45) Vielstich, W.; Lamm, A.; Gasteiger, H. A. *Handbook of Fuel Cells: Fundamentals, Technology, Applications*; Wiley: New York, **2003**.
- (46) Girishkumar, G.; Rettker, M.; Underhile, R.; Binz, D.; Vinodgopal, K.; McGinn, P.; Kamat, P. *Langmuir* **2005**, *21* (18), 8487–8494.
- (47) Antolini, E.; Salgado, J. R. C.; Gonzalez, E. R. *J. Power Sources* **2006**, *160* (2), 957–968.
- (48) Siracusano, S.; Stassi, A.; Baglio, V.; Arico, A. S.; Capitanio, F.; Tavares, A. C. *Electrochimica Acta* **2009**, *54* (21), 4844–4850.
- (49) Li, H. Q.; Sun, G. Q.; Li, N.; Sun, S. G.; Su, D. S.; Xin, Q. J. *J. Phys. Chem. C* **2007**, *111* (15), 5605–5617.
- (50) Pileni, M. P., *Nat. Mater.* **2003**, *2* (3), 145–150.
- (51) Son, S. U.; Jang, Y.; Yoon, K. Y.; Kang, E.; Hyeon, T. *Nano Lett.* **2004**, *4* (6), 1147–1151.
- (52) Seger, B.; Kamat, P. V. *J. Phys. Chem. C* **2009**, *113* (19), 7990–7995.
- (53) Xu, C.; Wang, X.; Zhu, J. W. *J. Phys. Chem. C* **2008**, *112* (50), 19841–19845.
- (54) Yoo, E.; Okata, T.; Akita, T.; Kohyama, M.; Nakamura, J.; Honma, I. *Nano Lett.* **2009**, *9* (6), 2255–2259.
- (55) Li, Y. J.; Gao, W.; Ci, L. J.; Wang, C. M.; Ajayan, P. M. *Carbon* **2010**, *48* (4), 1124–1130.
- (56) Gotoh, K.; Kawabata, K.; Fujii, E.; Morishige, K.; Kinumoto, T.; Miyazaki, Y.; Ishida, H. *Carbon* **2009**, *47* (8), 2120–2124.
- (57) Jin, Z.; Nackashi, D.; Lu, W.; Kittrell, C.; Tour, J. M. *Chem. Mater.* **2010**, *22* (20), 5695–5699.
- (58) Guo, S. J.; Dong, S. J.; Wang, E. W. *ACS Nano* **2010**, *4* (1), 547–555.
- (59) Dong, L. F.; Gari, R. R. S.; Li, Z.; Craig, M. M.; Hou, S. F. *Carbon* **2010**, *48* (3), 781–787.
- (60) Jalan, V.; Taylor, E. J. *J. Electrochem. Soc.* **1983**, *130* (11), 2299–2301.
- (61) Beard, B. C.; Ross, P. N. *J. Electrochem. Soc.* **1990**, *137* (11), 3368–3374.
- (62) Paffett, M. T.; Beery, J. G.; Gottesfeld, S. *J. Electrochem. Soc.* **1988**, *135* (6), 1431–1436.
- (63) Mukerjee, S.; Srinivasan, S.; Soriaga, M. P.; McBreen, J. *J. Electrochem. Soc.* **1995**, *142* (5), 1409–1422.
- (64) Min, M. K.; Cho, J. H.; Cho, K. W.; Kim, H. *Electrochim. Acta* **2000**, *45* (25–26), 4211–4217.
- (65) Qian, W.; Hao, R.; Zhou, J.; Eastman, Micah.; Manhat, B. A.; Sun, Q.; Goforth, A. M.; Jiao, J. *Carbon* **2013**, *52*, 595–604.
- (66) Sun, J. W.; Zhong, D. K.; Gamelin, D. R. *Energy Environ. Sci.* **2010**, *3* (9), 1252–1261.
- (67) Navarro, R. M.; Sanchez-Sanchez, M. C.; Alvarez-Galvan, M. C.; del Valle, F.; Fierro, J. L. G. *Energy Environ. Sci.* **2009**, *2* (1), 35–54.
- (68) Kudo, A.; Miseki, Y. *Chem. Soc. Rev.* **2009**, *38* (1), 253–278.
- (69) Hoffmann, M. R.; Martin, S. T.; Choi, W. Y.; Bahnemann, D. W. *Chem. Rev.* **1995**, *95* (1), 69–96.
- (70) Woan, K.; Pyrgiotakis, G.; Sigmund, W. *Adv. Mater.* **2009**, *21* (21), 2233–2239.
- (71) Yang, H. G.; Liu, G.; Qiao, S. Z.; Sun, C. H.; Jin, Y. G.; Smith, S. C.; Zou, J.; Cheng, H. M.; Lu, G. Q. *J. Am. Chem. Soc.* **2009**, *131* (11), 4078–4083.
- (72) Han, X. G.; Kuang, Q.; Jin, M. S.; Xie, Z. X.; Zheng, L. S. *J. Am. Chem. Soc.* **2009**, *131* (9), 3152–+.
- (73) Chae, S. Y.; Park, M. K.; Lee, S. K.; Kim, T. Y.; Kim, S. K.; Lee, W. I. *Chem. Mat.* **2003**, *15* (17), 3326–3331.
- (74) Zhang, Z. B.; Wang, C. C.; Zakaria, R.; Ying, J. Y. *J. Phys. Chem. B* **1998**, *102* (52), 10871–10878.
- (75) Wang, W. D.; Serp, P.; Kalck, P.; Faria, J. L. *Appl. Catal. B-Environ.* **2005**, *56* (4), 305–312.
- (76) Ou, Y.; Lin, J. D.; Fang, S. M.; Liao, D. W. *Chem. Phys. Lett.* **2006**, *429* (1–3), 199–203.
- (77) Fujishima, A.; Honda, K. *Nature* **1972**, *238* (5358), 37–+.
- (78) Oregan, B.; Gratzel, M. *Nature* **1991**, *353* (6346), 737–740.
- (79) Wijnhoven, J.; Vos, W. L. *Science* **1998**, *281* (5378), 802–804.
- (80) Yang, H. G.; Sun, C. H.; Qiao, S. Z.; Zou, J.; Liu, G.; Smith, S. C.; Cheng, H. M.; Lu, G. Q. *Nature* **2008**, *453* (7195), 638–U4.
- (81) Vittadini, A.; Selloni, A.; Rotzinger, F. P.; Gratzel, M. *Phys. Rev. Lett.* **1998**, *81* (14), 2954–2957.
- (82) Dai, Y. Q.; Cogley, C. M.; Zeng, J.; Sun, Y. M.; Xia, Y. N. *Nano Lett.* **2009**, *9* (6), 2455–2459.
- (83) Han, X. G.; Kuang, Q.; Jin, M. S.; Xie, Z. X.; Zheng, L. S. *J. Am. Chem. Soc.* **2009**, *131* (9), 3152–+.
- (84) Amano, F.; Prieto-Mahaney, O. O.; Terada, Y.; Yasumoto, T.; Shibayama, T.; Ohtani, B. *Chem. Mat.* **2009**, *21* (13), 2601–2603.
- (85) Chen, X.; Mao, S. S. *Chem. Rev.* **2007**, *107* (7), 2891–2959.
- (86) Zhang, H.; Lv, X. J.; Li, Y. M.; Wang, Y.; Li, J. H. *ACS Nano* **2010**, *4* (1), 380–386.
- (87) Zhang, X. Y.; Li, H. P.; Cui, X. L.; Lin, Y. H. *J. Mater. Chem.* **2010**, *20* (14), 2801–2806.
- (88) Williams, G.; Seger, B.; Kamat, P. V. *ACS Nano* **2008**, *2* (7), 1487–1491.
- (89) Liang, Y. Y.; Wang, H. L.; Casalongue, H. S.; Chen, Z.; Dai, H. J. *Nano Research* **2010**, *3* (10), 701–705.
- (90) Qian, W.; Fowler, S.; Greaney, A.; Chiu, S. K.; Goforth, A. M.; Jiao, J. *ACS Sustainable Chemistry & Engineering* **2014**, *2*, 1802–1810

## Graphene Nanocomposites

For a complete list of available materials, visit [aldrich.com/graphene](http://aldrich.com/graphene).

### Graphene-based Nanocomposites

10 mg/mL dispersion in acetone

Name	Particle Size (nm)	Composition	Prod. No.
Pt/graphene nanocomposite	2 - 5 (Pt nanocrystal)	acetone ~ 80 wt. % graphene 6-10% Pt nanoparticle 1-4%	<a href="#">803693-SML</a>
Pd/graphene nanocomposite	5 - 50 (Pd nanocrystal)	acetone ~ 80 wt. % graphene 6-10% Pd nanoparticle 2-6%	<a href="#">803707-SML</a>
PtPd/graphene nanocomposite	5 - 50 (PtPd nanocrystal)	acetone ~ 80% graphene 10-15% PtPd nanocrystal 5-10%	<a href="#">803758-SML</a>
PtCo/graphene nanocomposite	2 - 5 (PtCo nanocrystal)	acetone ~ 80% graphene 10-15% PtCo nanocrystal 5-10%	<a href="#">803766-SML</a>
Fe <sub>3</sub> O <sub>4</sub> /graphene nanocomposite	5 - 25 (Fe <sub>3</sub> O <sub>4</sub> nanocrystal)	acetone ~ 80 wt. % graphene 3-8% Fe <sub>3</sub> O <sub>4</sub> nanocrystal 4-9%	<a href="#">803715-SML</a>
Mn <sub>2</sub> O <sub>3</sub> /graphene nanocomposite	5 - 25 (Mn <sub>2</sub> O <sub>3</sub> nanocrystal)	acetone ~ 80 wt. % graphene 3-8% Mn <sub>2</sub> O <sub>3</sub> nanocrystal 4-9%	<a href="#">803723-SML</a>

## Reduced Graphene Oxide-based Nanocomposites

10 mg/mL dispersion in acetone

Name	Particle Size (nm)	Composition	Prod. No.
Pt/reduced graphene oxide nanocomposite	2 - 5 (Pt nanocrystal)	acetone ~ 80% reduced graphene oxide 5-20% Pt nanocrystal < 5%	803782-5ML
Pd/reduced graphene oxide nanocomposite	5 - 50 (Pd nanocrystal)	acetone ~ 80% reduced graphene oxide 5-20% Pd nanocrystal < 5%	803790-5ML
PtPd/reduced graphene oxide nanocomposite	5 - 50 (PtPd nanocrystal)	acetone ~ 80% reduced graphene oxide 10~18% PtPd nanocrystal 2~10%	803820-5ML
Fe <sub>3</sub> O <sub>4</sub> /reduced graphene oxide nanocomposite	5 - 25 (Fe <sub>3</sub> O <sub>4</sub> nanocrystal)	acetone ~ 80% reduced graphene oxide 10~17% Fe <sub>3</sub> O <sub>4</sub> nanocrystal < 3~8%	803804-5ML
Mn <sub>3</sub> O <sub>4</sub> /reduced graphene oxide nanocomposite	5 - 25 (Mn <sub>3</sub> O <sub>4</sub> nanocrystal)	acetone ~ 80% reduced graphene oxide 10~17% Mn <sub>3</sub> O <sub>4</sub> nanocrystal < 3~8%	803812-5ML
PtCo/Reduced Graphene Oxide Nanocomposite	2 - 5 (PtCo nanocrystal)	acetone ~ 80% reduced graphene oxide 10-18% PtCo nanocrystal 2-10%	803901-5ML

## Graphene

For a complete list of available materials, visit [aldrich.com/graphene](http://aldrich.com/graphene).

### Graphene and Graphene Nanoplatelets

Name	Form	Sheet Resistance	Prod. No.
Graphene dispersion	10 mg/mL, dispersion in NMP	<10 <sup>3</sup> Ω/sq (graphene)	803839-5ML
Graphene nanoplatelets	1 mg/mL, dispersion in H <sub>2</sub> O	10 (+/-5) Ω/sq (for a 25 μm film)	799092-50ML
Graphene nanoplatelets	powder	10 (+/-5) Ω/sq (for a 25 μm film)	799084-500MG

### Graphene Nanoribbons

Name	Purity (%)	Dimension	Surface Area	Prod. No.
Graphene nanoribbons, alkyl functionalized	≥85	L x W 2-15 μm x 40-250 nm	BET surf. area 38 m <sup>2</sup> /g	797766-500MG
Graphene nanoribbons	≥90.0	L x W 2-15 μm x 40-250 nm	BET surf. area 48-58 m <sup>2</sup> /g	797774-500MG

### Graphene Inks

Name	Descriptions	Prod. No.
Graphene dispersion	with ethyl cellulose in cyclohexanone and terpineol, inkjet printable	793663-5ML
Graphene dispersion	with ethyl cellulose in terpineol, gravure printable	796115-10ML
Graphene dispersion	with ethyl cellulose in terpineol, screen printable	798983-10ML

## HAVE YOU MISSED A RECENT ISSUE?

- Vol. 10 No. 1: 10<sup>th</sup> Anniversary Issue—Materials that Matter (RQ)
- Vol. 9 No. 4: Materials for Energy Harvesting and Storage (REO)
- Vol. 9 No. 3: Polymers in Therapeutics and Nanomedicine (QZP)
- Vol. 9 No. 2: Inorganic Materials in Biomedical Applications (QIV)
- Vol. 9 No. 1: Materials for Flexible and Printed Electronics (QFD)
- Vol. 8 No. 4: Materials for Energy Storage and Efficiency (PVS)

To view a complete library of issues or to subscribe to our newsletter, visit [aldrich.com/materialmatters](http://aldrich.com/materialmatters)



## Nanoparticles for Nanocomposites

For a complete list of available materials, visit [aldrich.com/nanoparticles](http://aldrich.com/nanoparticles).

Name	Size (nm)	Description	Form	Prod. No.
Cobalt(II,III) oxide	particle size <50 (TEM)	99.5% trace metals basis	nanopowder	637025-25G 637025-100G 637025-250G
Iron(III) oxide	particle size <50 (BET)	crystalline (primarily $\gamma$ )	nanopowder	544884-5G 544884-25G
Iron(II,III) oxide	particle size 50 - 100 (TEM)	97% trace metals basis	nanopowder spherical	637106-25G 637106-100G 637106-250G
Iron oxide(II,III), magnetic nanoparticles solution	avg. part. size 10 particle size 9 - 11 (TEM; conforms)	-	solution	700312-5ML
	avg. part. size 5 particle size $5 \pm 1$ nm (TEM; conforms)	-	solution	700320-5ML
	avg. part. size 20 particle size 18 - 22 (TEM)	-	solution	700304-5ML
Iron(III) oxide, dispersion	avg. part. size <30 (APS) particle size <100 (DLS)	-	nanoparticles	720704-100G
Magnesium oxide	particle size <50 (BET)	-	nanopowder	549649-5G 549649-25G
Titanium(IV) oxide, anatase	particle size <25	99.7% trace metals basis	nanopowder	637254-50G 637254-100G 637254-500G
Titanium(IV) oxide, mixture of rutile and anatase	particle size <50 (XRD) particle size <100 (BET)	99.5% trace metals basis	nanopowder	634662-25G 634662-100G
Titanium(IV) oxide, rutile	particle size <100, diam. $\times$ L $\sim$ 10 $\times$ $\sim$ 40 nm	99.5% trace metals basis	nanopowder	637262-25G 637262-100G 637262-500G
Titanium(IV) oxide, mixture of rutile and anatase	particle size <150 (volume distribution, DLS) particle size $\sim$ 21 (primary particle size of starting nanopowder)	99.5% trace metals basis	dispersion nanoparticles	700347-25G 700347-100G
Platinum	particle size <50 (TEM)	-	nanopowder	685453-100MG 685453-250MG
Platinum, nanoparticle dispersion	particle size 3	99.99% trace metals basis	dispersion nanoparticle	773875-25ML
Platinum	particle size 200 (SEM)	99.9%, metals basis	nanopowder	771937-250MG
Palladium	particle size <25 (TEM)	$\geq$ 99.5% trace metals basis	nanopowder	686468-500MG
Gold nanoparticles	diameter 200	reactant free stabilized suspension in 0.1 mM PBS	suspension	746657-25ML 746657-100ML
	diameter 150	reactant free stabilized suspension in 0.1 mM PBS	suspension	746649-25ML 746649-100ML
	diameter 400	reactant free stabilized suspension in 0.1 mM PBS	suspension	746681-25ML
	diameter 300	reactant free stabilized suspension in 0.1 mM PBS	suspension	746673-25ML
	diameter 250	reactant free stabilized suspension in 0.1 mM PBS	suspension	746665-25ML 746665-100ML
	diameter 10	dispersion in H <sub>2</sub> O silica coated	dispersion	747564-5ML
	diameter 20	dispersion in H <sub>2</sub> O silica coated	dispersion	747572-5ML
	diameter 5	dispersion in H <sub>2</sub> O silica coated	dispersion	747556-5ML

# GRAPHENE FIELD EFFECT TRANSISTORS FOR BIOLOGICAL AND CHEMICAL SENSORS



Victoria Tsai\* and Bruce Willner  
Graphene Frontiers, Philadelphia, PA 19104, USA  
\*Email: victoria@graphenefrontiers.com

## Introduction

The detection and quantification of biomarkers are essential for medical diagnostics, environmental monitoring, and bioresearch. This field has long been dominated by optically based readout techniques utilizing fluorescent markers or those requiring advanced spectroscopic equipment. While other fields have benefited from new technologies based upon advancements in semiconductor integrated circuit technology, chemical and biological sensors have remained dependent upon biochemical assays due to the challenges of achieving sensitivity and selectivity with semiconductor-based sensors. Silicon transistor-based readout sensors have been developed, but these devices suffered from poor sensitivity and selectivity due to fundamental shortcomings of the silicon structure.

Recently, new electronic sensors have overcome the limitations of the current silicon sensors through the development of low dimensional materials, nanowires, nanotubes, and two-dimensional (2D) films. While sensors based upon one-dimensional (1D) structures, specifically carbon nanotubes (CNTs), have demonstrated excellent sensitivity and at least the promise of selectivity, the production of devices from 1D structures has proven difficult. Graphene offers the same performance opportunities as 1D structures along with the advantages of working with a planar film.

## Graphene

Graphene, the first 2D atomic crystal material, is a monolayer of carbon arranged in a hexagonal lattice. Andre Geim and Konstantin Novoselov were awarded the Nobel Prize in Physics in 2010 for their groundbreaking experiments on graphene. Graphene has several exceptional material properties particularly well suited for sensor applications, including electrical conductivity.<sup>1-3</sup> Ideal mobilities for graphene are estimated to be  $200,000 \text{ cm}^2 \text{ V}^{-1} \text{ s}^{-1}$ .<sup>4</sup> Mobilities of  $10,000\text{--}15,000 \text{ cm}^2 \text{ V}^{-1} \text{ s}^{-1}$  have been reported for exfoliated graphene on  $\text{SiO}_2$ -covered silicon wafers,<sup>5,6</sup> and upper limits between  $40,000\text{--}70,000 \text{ cm}^2 \text{ V}^{-1} \text{ s}^{-1}$ .<sup>6,7</sup> Graphene is very stable; it is composed of very short, strong, covalent bonds, all in the plane of the

film. The conductivity, stability, uniformity, composition, and 2D nature of graphene make it an excellent material for sensors, overcoming the failings of silicon chemical and biological sensors.

## GFET

A graphene field effect transistor (GFET) is composed of a graphene channel between two electrodes with a gate contact to modulate the electronic response of the channel (**Figure 1**). The graphene is exposed to enable functionalization of the channel surface and binding of receptor molecules to the channel surface. The surface of the GFET channel is functionalized by binding receptor molecules for the specific target of interest.

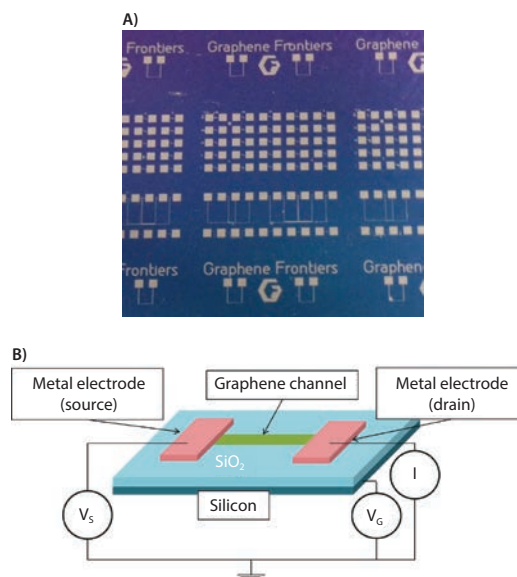


**Figure 1.** Graphene field effect transistors (GFET). **A)** Chips with 30 GFETs. **B)** Structure of GFET.

When a target molecule binds to the receptor on the graphene surface, the redistribution of electronic charge generates a change in the electric field across the FET channel region, which changes the electronic conductivity in the channel and the overall device response (**Figures 2,3**). Similar devices have been fabricated with silicon FETs for years, but achieved limited sensitivity and poor selectivity. Graphene generally does not react or bind with most materials; however, being composed of carbon, there are several chemistries that enable functionalization through formation of binding sites on the surface, discussed further in this section.

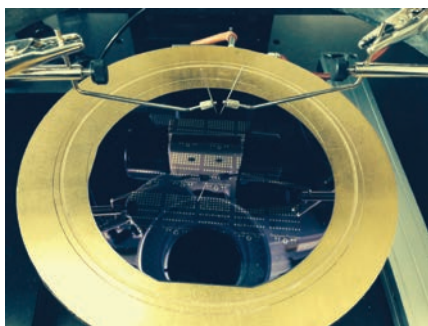


Figure 2. Probe station for recording GFET electrical measurements

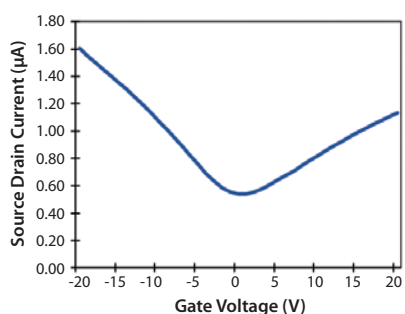


Figure 3. GFET device response as a function of gate voltage.

GFET sensors utilizing a 2D channel material have several advantages over bulk semiconductor devices (including silicon). For most semiconductor transistor sensors, local electric field changes at the channel surface have little effect deeper in the device channel, limiting the response sensitivity. With a GFET, the graphene channel is only one atom thick, meaning the entire channel is effectively on the surface and directly exposed to the environment. Any molecule attached to the surface of the channel impacts electronic transfer through the entire depth of the device. Near atomically thin silicon or other bulk semiconductors are not effective because at such a thickness, surface defects dominate the material characteristics. Two-dimensional materials, such as graphene, do not have surface dangling bonds to form defects. As a result, the graphene is highly conductive and sensitive to surface effects. Furthermore, since the material has no dangling bonds, it eliminates nonspecific binding and thus false positives, which has been an issue with other FET-based sensors. With the correct functionalization, GFETs enable highly sensitive, highly selective, direct, label-free detection of targeted analytes with an all-electronic device control and readout.

Graphene-based FET sensors have distinct fabrication advantages over devices fabricated with 1D materials, such as carbon nanotubes (CNTs) and nanowires. Like graphene, single wall CNTs are also highly conductive (with the correct chirality) and effectively all surface. Graphene can be produced in uniform films, with uniform material characteristics. Currently, 1D materials cannot be fabricated with the same consistency. Furthermore, arrays of high-yield, uniform response devices cannot be produced using randomly distributed nanowires or nanotubes because the number and orientation of the 1D objects vary across a distribution. This non-uniformity of position, often aggravated by non-uniformity of dimensions between 1D objects, creates a large variation of response characteristics between devices. 2D materials provide a route to achieve device-to-device consistency. Furthermore, uniform, wafer-scale graphene films can be formed by chemical vapor deposition, and these films are amenable to the photolithographic fabrication techniques developed for integrated circuit fabrication processes developed by the semiconductor industry.

## GFET Fabrication

GFETs are fabricated on silicon wafers to take advantage of the established, low-cost, highly reliable lithography, deposition, and integration processes of the integrated circuit industry. For these devices, graphene films were formed by atmospheric pressure chemical vapor deposition.<sup>8</sup> The copper foil deposition substrate was loaded into a furnace and heated to 1,000 °C in an argon/hydrogen reducing environment to remove any native oxide on the surface of the copper. A small flow of methane was added to the gas flow. Graphene formation begins with a few nucleation sites followed by lateral growth of the single atomic layer graphene crystals until the domains meet, completely coating the copper surface. The methane breaks down at the copper surface and the adsorbed carbon atoms travel on the surface until it meets up with and adds to the graphene crystals. Continuous single atomic layer graphene (SLG) was formed after a short growth time of 5 to 30 minutes, depending primarily upon the gas flow ratio.

Metal electrodes were deposited on a silicon wafer by thermal evaporation and patterned lithographically. The thin titanium or chromium layer is necessary for adhesion to the SiO<sub>2</sub> surface. Gold or palladium provides the electronic contact with the graphene. The graphene film was transferred from the copper deposition substrate and overlaid on the wafer after the formation of the electrodes. To perform the transfer, Poly(methyl methacrylate) (PMMA, Aldrich Prod. Nos. 182230, 445746, and 182265) was spincoated on the graphene face of the copper substrate. The copper was separated from the PMMA/graphene by a mechanical separation with water electrolysis. The graphene film was placed on the wafer surface, the wafer was baked to promote adhesion of the graphene to the wafer and electrodes, and the PMMA was removed with acetone. Additional photolithography was used to pattern the graphene into FET channels between electrodes, and oxygen plasma was effective at removing unprotected graphene. The minimization of metal contaminants in graphene films is critical for integration in the IC fabrication facilities. Avoiding processes which etch away the copper substrate is essential to achieve this.

## GFET Functionalization

Over the past few years, a number of well-controlled chemical functionalization procedures have been developed that are compatible with GFETs. Graphene FETs have been functionalized with proteins, chemical compounds, and DNA molecules to make sensors for various applications.

For the case of protein functionalization, non-specific protein binding is undesirable as it typically implies loss of control over the protein's functional structure.<sup>9</sup> A.T. Charlie Johnson's group at the University of Pennsylvania has demonstrated multiple attachment chemistries appropriate for use on graphene devices. These can be based on diazonium compounds that form a covalent bond to the graphene surface<sup>10</sup> or bifunctional pyrene compounds that interact with graphene through a  $\pi$ - $\pi$  stacking interaction.<sup>10,11</sup> The linkage to the protein can be done through amide bond that is permitted at suitable amine groups on the protein exterior<sup>11</sup> or via Ni-nitritriacetic acid linkage to a histidine tag on a recombinant protein.<sup>12</sup> In each case, control of the parameters of the attachment chemistry (e.g., concentration, temperature, time) make it possible to perform the functionalization while retaining the high quality properties of the graphene device that contribute to high sensitivity (in particular, the high carrier mobility and favorable noise characteristics).

## Applications in Biosensors and Chemical Sensors

Graphene's exceptional electronic and thermal properties and high surface to volume ratio make it particularly suited in applications such as biosensors,<sup>13,14</sup> gas sensors,<sup>15,16</sup> and high performance transistors.<sup>17–19</sup> Graphene-based devices could enable rapid high-sensitivity sensors for healthcare point-of-care diagnostics and chemical detection and have the potential to replace other methodologies that are high cost, low sensitivity, and labor intensive.

A.T. Charlie Johnson's group has demonstrated a GFET sensor for the detection of small molecules at pg/mL concentrations.<sup>14</sup> GFETs were functionalized with a computationally designed water-soluble variant of human  $\mu$ -opioid receptor (G protein-coupled receptor) using the 4-carboxybenzenediazonium tetrafluoroborate, which produced carboxylic acid sites on the graphene, which were further activated and stabilized with 1-ethyl-3-[3-dimethylaminopropyl] carbodiimide hydrochloride (**Sigma Prod. No. 03449** and **Sigma-Aldrich Prod. No. E7750**)/sulfo-N-hydroxysuccinimide (EDC/sNHS).<sup>20</sup> Electronic measurements of the source-drain current as a function of the back-gate voltage following each step of the functionalization procedure showed reproducible shifts in conductance. Detection of the  $\mu$ -opioid receptor target naltrexone (opioid receptor antagonist, **Fluka Prod. No. 1453504**) was reported at concentrations as low as 10 pg/mL, with high specificity.<sup>14</sup> Studies utilizing engineered single chain variable fragment (scFv) instead of full antibodies as receptor molecules on other carbon-based FET sensors have shown a 1,000x improvement in the detection limit.<sup>21</sup> scFv is an engineered fusion protein containing the variable regions of the antibody which are specific to the antigen and retain the specificity of the original antibody despite the removal of the constant regions which make up the majority of the antibody. The improved sensitivity of FET sensors functionalized with scFvs can be attributed to the closer proximity of the bound biomarker target to the GFET channel, thus leading to stronger electrostatic interactions and a larger electrical signal.<sup>21</sup>

Chemical vapor sensing, or "noselike" vapor sensing, is another application that uses GFETs. To do this, GFETs were functionalized with single-stranded DNA to detect various chemical vapors. The GFET-based chemical sensors showed fast response times, rapid recovery to baseline at room temperature, and discrimination between several similar vapor analytes: e.g., dimethyl methylphosphonate (DMMP, **Aldrich Prod. No. D169102**) and propionic acid (**Sigma-Aldrich Prod. No. 402907**).<sup>16</sup>

## Conclusions and Future Outlook

Graphene's exceptional electronic properties continue to hold high promise in sensing applications. GFET-based sensors for biological and chemical applications would enable rapid, sensitive, specific, low-cost, and all-electronic readouts. Furthermore, the GFET sensors can be multiplexed, thus making it possible to rapidly test for multiple targets (tens to thousands) with high sensitivity on a single small-sized chip. GFET sensor technology will have the potential to disrupt healthcare, drug discovery, and chemical detection markets.

### References

- Novoselov, K. S. et al. A roadmap for graphene. *Nature* **2012**, *490*, 192–200, doi:10.1038/nature11458.
- Geim, A. K.; Novoselov, K. S. The rise of graphene. *Nature materials* **2007**, *6*, 183–191, doi:nmat1849 [pii] 10.1038/nmat1849.
- Geim, A. K. Graphene: status and prospects. *Science* **2009**, *324*, 1530–1534, doi:10.1126/science.1158877.
- Bolotin, K. I. et al. Ultrahigh electron mobility in suspended graphene. *Solid State Communications* **2008**, *146*, 351–355.
- Novoselov, K. S. et al. Electric field effect in atomically thin carbon films. *Science* **2004** *306*, 666–669, doi:10.1126/science.1102896.
- Chen, J.-H.; Jang, C.; Xiao, S.; Ishigami, M.; Fuhrer, M. S. Intrinsic and extrinsic performance limits of graphene devices on SiO<sub>2</sub>. *Nature nanotechnology* **2008**, *3*, 206–209.
- Chen, F.; Xia, J.; Ferry, D. K.; Tao, N. Dielectric screening enhanced performance in graphene FET. *Nano Lett.* **2009**, *9*, 2571–2574, doi:10.1021/nl900725u.
- Luo, Z. et al. Effect of Substrate Roughness and Feedstock Concentration on Growth of Wafer-Scale Graphene at Atmospheric Pressure. *Chemistry of Materials* **2011**, *23*.
- Alava, T. et al. Control of the graphene-protein interface is required to preserve adsorbed protein function. *Analytical chemistry* **2013**, *85*, 2754–2759, doi:10.1021/ac303268z.
- Lu, Y. et al. Graphene-Protein Bioelectronic Devices with Wavelength-Dependent Photoresponse. *Applied Physics Letters* **2012**, *100*.
- Lerner, M. B. et al. Toward quantifying the electrostatic transduction mechanism in carbon nanotube molecular sensors. *Journal of the American Chemical Society* **2012**, *134*, 14318–14321, doi:10.1021/ja306363v.
- Goldsmith, B. R. et al. Biomimetic chemical sensors using nanoelectronic readout of olfactory receptor proteins. *ACS Nano* **2011**, *5*, 5408–5416, doi:10.1021/nn200489j.
- Wang, Y.; Shao, Y.; Matson, D. W.; Li, J. & Lin, Y. Nitrogen-doped graphene and its application in electrochemical biosensing. *ACS Nano* **2010**, *4*, 1790–1798, doi:10.1021/nn100315s.
- Lerner, M. B. et al. Scalable production of highly sensitive nanosensors based on graphene functionalized with a designed G protein-coupled receptor. *Nano Lett.* **2014**, *14*, 2709–2714, doi:10.1021/nl5006349.
- Schedin, F. et al. Detection of individual gas molecules adsorbed on graphene. *Nature materials* **2007**, *6*, 652–655, doi:10.1038/nmat1967.
- Lu, Y.; Goldsmith, B. R.; Kybert, N. J. & Johnson, A. T. C. DNA-decorated graphene chemical sensors. *Applied Physics Letters* **2010**, *97*.
- Wu, Y. et al. High-frequency, scaled graphene transistors on diamond-like carbon. *Nature* **2011**, *472*, 74–78, doi:10.1038/nature09979.
- Liao, L. et al. High-speed graphene transistors with a self-aligned nanowire gate. *Nature* **2010**, *467*, 305–308, doi:10.1038/nature09405.
- Lin, Y. M. et al. 100-GHz transistors from wafer-scale epitaxial graphene. *Science* **2010**, *327*, 662, doi:10.1126/science.1184289.
- Lerner, M. B., Dailey, J., Goldsmith, B. R., Brisson, D. & Johnson, A. T. Detecting Lyme disease using antibody-functionalized single-walled carbon nanotube transistors. *Biosens Bioelectron* **2013**, *45*, 163–167, doi:10.1016/j.bios.2013.01.035.
- Lerner, M. B. et al. Hybrids of a genetically engineered antibody and a carbon nanotube transistor for detection of prostate cancer biomarkers. *ACS Nano* **2012**, *6*, 5143–5149, doi:10.1021/nn300819s.

## Graphene Field Effect Transistor Chips

For a complete list of available materials, visit [aldrich.com/graphene](http://aldrich.com/graphene).

Name	Graphene Information	Resistance	GFET Device Information	Prod. No.
Graphene field effect transistor chip	Material uniformity: >95% Single layer graphene FET mobility on Al <sub>2</sub> O <sub>3</sub> : ~3,000 cm <sup>2</sup> /V sec FET mobility on Si/SiO <sub>2</sub> : ~1,500 cm <sup>2</sup> /V sec	900 ± 50 Ω/sq on Si/SiO <sub>2</sub>	GFET Device Dirac Voltage Range: 0-60V 10 devices per chip	<b>803995-1EA</b>

## Graphene Films

For a complete list of available materials, visit [aldrich.com/graphene](http://aldrich.com/graphene).

Name	Sheet Resistance	Prod. No.
Monolayer graphene film, 1 cm x 1 cm on copper foil	600 $\Omega$ /sq	773697-4EA
Monolayer graphene film, 1 in. x 1 in. on copper foil	350 $\Omega$ /sq	799009-1EA
Monolayer graphene film, 1 cm x 1 cm on quartz	600 $\Omega$ /sq	773719-4EA
Monolayer graphene film, 1 cm x 1 cm on SiO <sub>2</sub> /Si substrate	600 $\Omega$ /sq	773700-4EA
Monolayer graphene film, 1 in. x 1 in. on PET film	700 $\Omega$ /sq	745863-1EA 745863-5EA
Monolayer graphene film, 2 in. x 2 in. on PET film	700 $\Omega$ /sq	745871-1EA
Suspended monolayer graphene on TEM grid substrate (Quantifoil gold)	170 $\Omega$ /sq	798177-1PK

**ALDRICH**  
Materials Science

# MATERIALS FOR INNOVATION

### BIOMEDICAL

Materials for drug delivery, tissue engineering, and regenerative medicine; PEGs, biodegradable and natural polymers; functionalized nanoparticles; block copolymers, dendrimers and nanoclays

### ELECTRONICS

Nanowires; printed electronics inks and pastes; materials for OPV, OFET, OLED; nanodispersions; CNTs and graphene; precursors for PVD, CVD, and sputtering

### ENERGY

Ready-to-use battery grade electrode and electrolyte materials; nanopowders, nanostructures and dispersions; quantum dots; perovskites; fuel cells and membrane; hydrogen storage materials including MOFs; phosphors; thermoelectrics; high purity salts

Find more information on our capabilities at  
[aldrich.com/matsci](http://aldrich.com/matsci)

# FLUORESCENCE QUENCHING MICROSCOPY: IMAGING TWO-DIMENSIONAL MATERIALS



Alane Lim and Jiaxing Huang\*  
Department of Materials Science and Engineering,  
Northwestern University, Evanston, IL 60208, USA  
\*Email: jiaxing-huang@northwestern.edu

## Introduction

Developed in the last several years, fluorescence quenching microscopy (FQM)<sup>1–3</sup> has enabled rapid, inexpensive, and high-fidelity visualization of two-dimensional (2D) materials such as graphene-based sheets (Aldrich Prod. Nos. 763713, 794341 and 777684) and MoS<sub>2</sub> (Aldrich Prod. Nos. 234842 and 69860). Graphene and other emerging 2D materials have attracted considerable interest in recent years due to their novel properties and exciting applications,<sup>4</sup> but the characterization of these materials has remained challenging. In conventional fluorescence microscopy, imaging is enabled by fluorescent labeling, where excitation makes the targets lighten up against a dark background. However, this approach becomes less effective when the objects of interest are strong fluorescence quenchers, such as graphite and graphene-based sheets.<sup>1,5,6</sup> FQM-based techniques use a reverse approach, where a fluorescent layer is applied to cover both the targets and their surrounding area. Upon excitation, graphene-based sheets appear dark against a bright background. The long-range fluorescence quenching capability of 2D materials<sup>1–3,5</sup> also makes it possible to differentiate overlapping layers, wrinkles, and folds because they appear darker than single layers. Thus, FQM is capable of producing crisp images with contrast and layer resolution, comparable to those obtained from atomic force microscopy (AFM) and scanning electron microscopy (SEM). A further advantage of FQM is its flexibility in different formats: capable of imaging 2D sheets on arbitrary substrates and in solution.

## Basic Principles of Imaging 2D Materials by FQM

Graphene-based sheets quench the fluorescence of dye molecules through either long-range energy transfer mediated by dipole–dipole interactions or short-range electron/charge transfer. The charge transfer mechanism requires orbital overlap, and is, thus, limited within the distance of molecular contact. In contrast, dipole–dipole interactions can extend over much longer distances through empty or even occupied space.<sup>7</sup> Although both mechanisms lead to fluorescence quenching, only the long-range mechanism, which is essentially Förster resonance energy transfer (FRET), is suitable for FQM as it enables contrast between different numbers of layers.<sup>1–3,8</sup> Signal contrast in an FQM measurement is generated through the difference in fluorescence quenching between the sample of interest and the substrate (which is quite generic to all materials). Since the lateral resolution of FQM is diffraction limited, when performed using a standard optical microscope, FQM is especially well-suited for imaging objects with micron-scale lateral dimensions such as graphene sheets, graphene oxide, and flakes of other 2D materials.

## Methods and Procedures of FQM

FQM samples can be conveniently prepared by spin-coating a dye-doped polymer layer onto a substrate (Figure 1A). A polymer is added to produce a uniform thin film, upon which a fluorescent dye is dispersed to enable imaging. Due to the broadband quenching capability of graphene-based sheets, FQM is not limited by the wavelength of illumination and can be performed using a wide range of fluorescent materials. Therefore, a great number of dye/polymer combinations can be used based on their processability in different solvents, as well as their capability of forming thin films. For example, fluorescein (Sigma Prod. No. 46955)/polyvinylpyrrolidone (Aldrich Prod. Nos. 234257, 856568 and 437190) (FL/PVP) can be processed in water or ethanol, and 4-(dicyanomethylene)-2-methyl-6-(4-dimethylaminostyryl)-4H-pyran (Aldrich Prod. No. 410497)/poly(methyl methacrylate) (Aldrich Prod. Nos. 182230, 445746, etc.) (DCM/PMMA) can be processed in organic solvents such as chloroform (Sigma-Aldrich Prod. No. 437581, etc.), toluene (Sigma-Aldrich Prod. No. 179418, etc.), and anisole (Sigma-Aldrich Prod. Nos. 123226 and 296295). The fluorescent layer can be either on top of the sample or beneath it. The thickness of the dye/polymer layer affects the contrast of FQM images. Dye layer thickness in

the range of tens of nanometers has been shown to produce the highest quality FQM images, achieving high contrast and the ability to resolve different numbers of layers. **Figure 1B** is an FQM image of graphene oxide (GO) sheets deposited on a glass coverslip taken with a digital camera directly through an eyepiece of a fluorescence microscope. This image represents the naked-eye view under FQM. Note that if the substrate itself is fluorescent, one can take advantage of such auto-fluorescence to perform FQM directly without any additional dye layer.

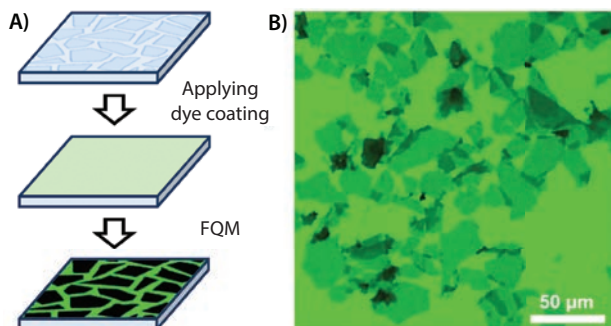


**Figure 1.** A) FQM can be conveniently performed by applying a dye coating on samples deposited on an arbitrary substrate. B) A naked-eye view of GO sheets on a glass coverslip, obtained with a digital camera directly through an eyepiece of the microscope, showing vivid contrast between different numbers of layers. Wrinkles, folds, and overlaps can be clearly seen. The dye layer was FL/PVP. Reproduced with permission from Reference 1, copyright American Chemical Society.

FQM offers significant advantages over the three most commonly used microscopy methods for imaging 2D materials: reflectance mode of optical microscopy, atomic force microscopy (AFM), and scanning electron microscopy (SEM). All of these techniques are limited to 2D sheets deposited on specific substrates. Reflectance-mode optical microscopy can only produce sufficient contrast using samples deposited on specific types of Si wafers. Meanwhile, AFM is a very low throughput metrology method and can only image small sample areas on molecularly smooth substrates. SEM requires sheets be deposited on conductive substrates and can only be performed under vacuum. In contrast, FQM can tolerate significant surface roughness compared to AFM and reflectance spectroscopy and works on a wide variety of substrates, including metal, glass, and plastic. While previously it has been difficult to image graphene and related 2D materials on glass or plastic substrates, FQM finally allows for rapid microscopy of these 2D sheets using common chemicals and lab supplies.

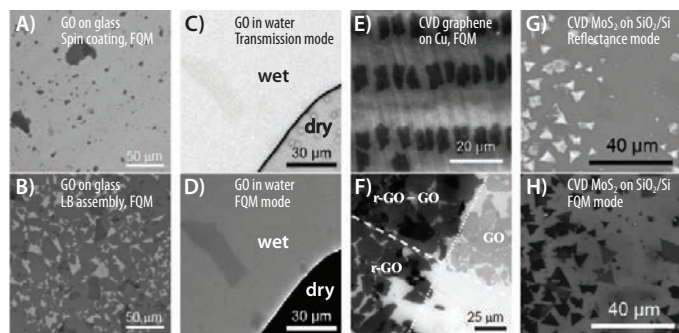


**Figure 2.** FQM images of GO sheets (Aldrich Prod. No. 763705) deposited on coverslip by (A) spin coating and (B) LB assembly. Optical microscopy images of GO sheets suspended in fluorescein solution acquired by (C) transmission and (D) FQM modes. E) An FQM image showing CVD graphene flakes grown on Cu foil. F) FQM can readily differentiate graphene-based sheets with different degrees of graphitization. Optical microscopy images of CVD grown MoS<sub>2</sub> sheets on SiO<sub>2</sub>/Si substrate acquired by (G) reflectance and (H) FQM modes. The thinnest sheets are more visible in the FQM image. C–D) are reproduced with permission from Reference 1, copyright American Chemical Society. F–H) are reproduced with permission from Reference 3, copyright John Wiley & Sons, Inc.

## Capabilities of FQM

Due to its ease of use and low cost, FQM has already been adopted by many research groups for characterization of graphene-based sheets. FQM is particularly suited for quickly checking the morphology of a sample or thin film, a task that has previously required analysis using SEM. Since FQM is capable of producing high quality images comparable to those obtained by SEM (but on much cheaper substrates like coverslips), it can replace SEM for the routine imaging of many micron-sized sheets. In fact, at Northwestern University, FQM has been incorporated into one of the undergraduate lab modules, where students use the technique to determine how processing techniques of graphene-based sheets impact final thin film microstructures. **Figures 2A–B** show FQM images of GO sheets deposited on glass coverslips by spin coating and Langmuir-Blodgett (LB) assembly,<sup>9</sup> respectively. Other than the obvious difference in coverage, the spin coated sample contains a significantly higher fraction of small GO pieces than the LB sample. This is due to the size-dependent amphiphilicity of GO.<sup>10–12</sup> Smaller sheets have higher charge density and are more hydrophilic, making them less likely to remain on the water surface during LB assembly. FQM also allows for the direct visualization of GO sheets in water. **Figure 2D** is an FQM image that clearly shows a GO sheet suspended in an aqueous fluorescein solution that is barely visible under transmission mode (**Figure 2C**). This capability, which allows for the real-time observation of how GO sheets are manipulated by capillary action during dewetting, inspired our discovery of crumpled, paper-ball like graphene by an aerosol-based synthetic route.<sup>8,13</sup> As mentioned earlier, FQM is generally applicable as long as there is a detectable difference of fluorescence quenching capability between the sample and substrate. Therefore, FQM can even visualize graphene deposited on metal surfaces, which themselves are strong quenchers. One example, **Figure 2E**, shows graphene flakes grown on Cu foil (Aldrich Prod. No. 773697) by chemical vapor deposition (CVD).<sup>3</sup> Another niche capability of FQM is that it can very easily generate contrast between graphene samples with different degrees of graphitization. The FQM image in **Figure 2F** shows very strong contrast between GO and reduced GO (r-GO), which is more graphitic because r-GO quenches fluorescence more strongly than GO.<sup>1</sup> This capability has proven very useful for visualizing graphene patterns or circuits created by writing the insulating sp<sup>3</sup> domains on graphene sheets.<sup>14</sup> Most recently, FQM has also been extended to visualize MoS<sub>2</sub> sheets (**Figures 2G–H**).<sup>3</sup>

Concerns have been raised that the dye/polymer coating used for FQM may introduce extra processing steps and possible sources of contamination to the sample. For most routine sample testing needs, however, this is not an issue since most samples are not subject to further experimentation after microscopy. Even for applications that involve further experimentation on the same sample, FQM can be readily integrated into the existing processing steps without introducing additional difficulty, and may even enable new capabilities. For example, a layer of PMMA is often applied to CVD-grown graphene samples to remove them from the metal foil substrate, which can be used to form the fluorescence layer for FQM. Similarly, device fabrication usually involves coating the sample with a polymeric layer of photoresist or e-beam resist, which can be used for the purpose of FQM as well. In fact, this allows sheet-specific projection lithography to first select a flake and then perform photolithography of the same flake under a fluorescence microscope.<sup>2</sup> Finally, since the dye is dispersed in the polymer layer, there are only a very limited number of dye molecules in contact with the 2D sheets. At least for the FL/PVP system, the fluorescent layer can be conveniently washed off by water and ethanol, without interrupting and contaminating the underlying sheets.<sup>1</sup>

## Acknowledgments

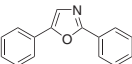
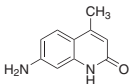
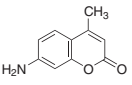
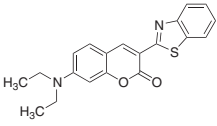
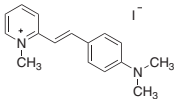
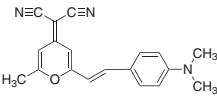
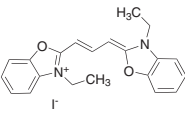
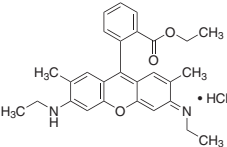
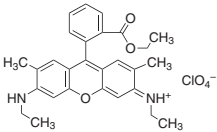
This work was supported by the National Science Foundation through a CAREER award (DMR 0955612).

### References

- (1) Kim, J.; Cote, L. J.; Kim, F.; Huang, J. X. *J. Am. Chem. Soc.* **2010**, *132*, 260–267.
- (2) Kim, J.; Kim, F.; Huang, J. X. *Mater. Today* **2010**, *13*, 28–38.
- (3) Tan, A. T. L.; Kim, J.; Huang, J. K.; Li, L. J.; Huang, J. X. *Small* **2013**, *9*, 3253–3258.
- (4) Butler, S. Z.; Hollen, S. M.; Cao, L. Y.; Cui, Y.; Gupta, J. A.; Gutierrez, H. R.; Heinz, T. F.; Hong, S. S.; Huang, J. X.; Ismach, A. F.; Johnston-Halperin, E.; Kuno, M.; Plashnitsa, V. V.; Robinson, R. D.; Ruoff, R. S.; Salahuddin, S.; Shan, J.; Shi, L.; Spencer, M. G.; Terrones, M.; Windl, W.; Goldberg, J. E. *ACS Nano* **2013**, *7*, 2898–2926.
- (5) Swathi, R. S.; Sebastian, K. L. *J. Chem. Phys.* **2009**, *130*.
- (6) Kagan, M. R.; Mccreery, R. L. *Anal. Chem.* **1994**, *66*, 4159–4165.
- (7) Turro, N. J.; Ramamurthy, V.; Scaiano, J. C. *Principles of molecular photochemistry: An introduction*; University Science Books: Sausalito, Calif., **2009**.
- (8) Luo, J. Y.; Kim, J.; Huang, J. X. *Acc. Chem. Res.* **2013**, *46*, 2225–2234.
- (9) Cote, L. J.; Kim, F.; Huang, J. X. *J. Am. Chem. Soc.* **2009**, *131*, 1043–1049.
- (10) Kim, F.; Cote, L. J.; Huang, J. X. *Adv. Mater.* **2010**, *22*, 1954–1958.
- (11) Kim, J.; Cote, L. J.; Kim, F.; Yuan, W.; Shull, K. R.; Huang, J. X. *J. Am. Chem. Soc.* **2010**, *132*, 8180–8186.
- (12) Cote, L. J.; Kim, J.; Tung, V. C.; Luo, J. Y.; Kim, F.; Huang, J. X. *Pure Appl. Chem.* **2011**, *83*, 95–110.
- (13) Luo, J. Y.; Jang, H. D.; Sun, T.; Xiao, L.; He, Z.; Katsoulidis, A. P.; Kanatzidis, M. G.; Gibson, J. M.; Huang, J. X. *ACS Nano* **2011**, *5*, 8943–8949.
- (14) Sun, Z. Z.; Pint, C. L.; Marcano, D. C.; Zhang, C. G.; Yao, J.; Ruan, G. D.; Yan, Z.; Zhu, Y.; Hauge, R. H.; Tour, J. M. *Nat. Commun.* **2011**, *2*, 559.

## Fluorescent Dyes

For a complete list of available materials, visit [aldrich.com/laserdye](http://aldrich.com/laserdye).

Structure	Name	Purity (%)	Absorption	Prod. No.
	2,5-Diphenyloxazole	99	$\lambda_{\text{max}} = 303 \text{ nm}$	D210404-25G D210404-100G D210404-500G
	Carbostyryl 124	99	$\lambda_{\text{max}} = 350 \text{ nm}$	363308-100MG 363308-500MG
	7-Amino-4-methylcoumarin	99	$\lambda_{\text{max}} = 354 \text{ nm}$	257370-100MG 257370-500MG
	Coumarin 6	98	$\lambda_{\text{max}} = 444 \text{ nm}$	442631-1G 442631-5G
	2-[4-(Dimethylamino)styryl]-1-methylpyridinium iodide	Dye content 95	$\lambda_{\text{max}} = 466 \text{ nm}$	280135-5G
	4-(Dicyanomethylene)-2-methyl-6-(4-dimethylaminostyryl)-4H-pyran	Dye content 98	$\lambda_{\text{max}} = 468 \text{ nm}$	410497-250MG 410497-1G
	3,3'-Diethyloxycarbocyanine iodide	98	$\lambda_{\text{max}} = 483 \text{ nm}$	320684-1G
	Rhodamine 6G	Dye content 99	$\lambda_{\text{max}} = 524 \text{ nm}$	252433-250MG 252433-1G
	Rhodamine 6G perchlorate	Dye content 99	$\lambda_{\text{max}} = 528 \text{ nm}$	252441-250MG 252441-1G

Structure	Name	Purity (%)	Absorption	Prod. No.
	Sulforhodamine B, acid form	Dye content 95	$\lambda_{\text{max}} = 558 \text{ nm}$	341738-1G 341738-5G
	3,3'-Diethylthiacarbocyanine iodide	Dye content 95	$\lambda_{\text{max}} = 560 \text{ nm}$	173738-250MG 173738-1G
	Styryl 9M	Dye content ~98	$\lambda_{\text{max}} = 584 \text{ nm}$	417025-1G
	Oxazine 170 perchlorate	Dye content 95	$\lambda_{\text{max}} = 624 \text{ nm}$	372056-100MG 372056-500MG
	Nile Blue A perchlorate	Dye content 95	$\lambda_{\text{max}} = 628 \text{ nm}$	370088-1G 370088-5G

## Poly(methyl methacrylate)

For a complete list of available materials, visit [aldrich.com/pmna](http://aldrich.com/pmna).

Structure	Average $M_w$	Prod. No.
	~15,000 by GPC	200336-50G 200336-100G
	~120,000 by GPC	182230-25G 182230-500G 182230-1KG
	~350,000 by GPC	445746-25G 445746-500G 445746-1KG
	~996,000 by GPC	182265-25G 182265-500G 182265-1KG

## Polyvinylpyrrolidone

For a complete list of available materials, visit [aldrich.com/pvp](http://aldrich.com/pvp).

Structure	Average $M_w$	Prod. No.
	~29,000	234257-5G 234257-100G 234257-500G
	~55,000	856568-100G 856568-500G 856568-10KG
	~1,300,000 by LS	437190-25G 437190-500G 437190-1KG

# MATERIALS RESEARCH SOCIETY MID-CAREER RESEARCHER AWARD

## Dr. Seth R. Marder Receives the 2015 Materials Research Society (MRS) Mid-Career Researcher Award

Dr. Seth R. Marder was named recipient of this award "for establishing fundamental relationships between the chemical structure of organic molecules and their optical and electronic properties, thereby profoundly impacting how the scientific community designs optimized molecular structures for use in nonlinear optical applications." The MRS Mid-Career Researcher Award, endowed by Aldrich® Materials Science, recognizes exceptional achievements in materials research made by mid-career professionals.

### About Dr. Marder

Dr. Marder received his Ph.D. in chemistry from the University of Wisconsin–Madison, has published over 375 peer-reviewed papers, and has been issued 23 patents, of which 11 are licensed and 9 were jointly developed with companies. Other honors include the Materials Awards from the Georgia Tech Research Corporation for Excellence in Research, American Chemical Society Arthur C. Cope Scholar, and the Outstanding Award in Research Program Development from Georgia Institute of Technology. Marder is a Fellow of the American Association for the Advancement of Science, the Optical Society of America, Society of Photo-Optical Instrumentation Engineers, the Royal Society of Chemistry, and the American Physical Society.



**Dr. Seth R. Marder**

Professor and Georgia Power Chair in the School of Chemistry and Biochemistry and the School of Materials Science and Engineering at the Georgia Institute of Technology

Find more information, visit  
[aldrich.com/mrsaward](http://aldrich.com/mrsaward)